

Virtual discovery of melatonin receptor ligands to modulate circadian rhythms

<https://doi.org/10.1038/s41586-020-2027-0>

Received: 3 August 2019

Accepted: 31 January 2020

Published online: 10 February 2020

 Check for updates

Reed M. Stein^{1,11}, Hye Jin Kang^{2,11}, John D. McCorvy^{2,9,11}, Grant C. Glatfelter^{3,10,11}, Anthony J. Jones³, Tao Che², Samuel Slocum², Xi-Ping Huang², Olena Savych⁴, Yurii S. Moroz^{5,6}, Benjamin Stauch^{7,8}, Linda C. Johansson^{7,8}, Vadim Cherezov^{7,8}, Terry Kenakin², John J. Irwin¹, Brian K. Shoichet^{1,12}✉, Bryan L. Roth^{2,12}✉ & Margarita L. Dubocovich^{3,12}✉

The neuromodulator melatonin synchronizes circadian rhythms and related physiological functions through the actions of two G-protein-coupled receptors: MT₁ and MT₂. Circadian release of melatonin at night from the pineal gland activates melatonin receptors in the suprachiasmatic nucleus of the hypothalamus, synchronizing the physiology and behaviour of animals to the light–dark cycle^{1–4}. The two receptors are established drug targets for aligning circadian phase to this cycle in disorders of sleep^{5,6} and depression^{1–4,7–9}. Despite their importance, few *in vivo* active MT₁-selective ligands have been reported^{2,8,10–12}, hampering both the understanding of circadian biology and the development of targeted therapeutics. Here we docked more than 150 million virtual molecules to an MT₁ crystal structure, prioritizing structural fit and chemical novelty. Of these compounds, 38 high-ranking molecules were synthesized and tested, revealing ligands with potencies ranging from 470 picomolar to 6 micromolar. Structure-based optimization led to two selective MT₁ inverse agonists—which were topologically unrelated to previously explored chemotypes—that acted as inverse agonists in a mouse model of circadian re-entrainment. Notably, we found that these MT₁-selective inverse agonists advanced the phase of the mouse circadian clock by 1.3–1.5 h when given at subjective dusk, an agonist-like effect that was eliminated in MT₁- but not in MT₂-knockout mice. This study illustrates the opportunities for modulating melatonin receptor biology through MT₁-selective ligands and for the discovery of previously undescribed, *in vivo* active chemotypes from structure-based screens of diverse, ultralarge libraries.

The recent determination of the crystal structures of the MT₁ and MT₂ receptors^{13,14} afforded us the opportunity to seek previously undescribed chemotypes with new functions, including MT₁-selective ligands, by computational docking of an ultralarge make-on-demand library¹⁵, seeking molecules that complemented the main ligand-binding (orthosteric) site of the receptor. Given the similarity of the MT₁ and MT₂ sites—in which 20 out of 21 residues are identical—and the challenges of docking for selectivity¹⁶, we sought to prioritize previously undescribed, high-ranking chemotypes from the docking screen that were unrelated to known melatonin receptor ligands and expected that these molecules interacted differentially with the two melatonin receptor types^{17–19}.

We docked more than 150 million ‘lead-like’ molecules, characterized by favourable physical properties from ZINC (<http://zinc15.docking.org>)^{15,20}. These largely make-on-demand molecules have not previously

been synthesized, but are usually accessible by two-component reactions. Use of complex building blocks in these reactions biases towards diverse, structurally interesting molecules^{15,20}. Each library molecule was sampled in an average of more than 1.6 million poses (orientations × conformations) in the MT₁ orthosteric site¹³ by DOCK3.7²¹, generating more than 72 trillion complexes for the library overall and scoring each pose for physical complementarity to the receptor site²¹. Seeking diversity, the top 300,000 scoring molecules were clustered by topological similarity, resulting in 65,323 clusters, and those that were similar to known MT₁ and MT₂ ligands from ChEMBL23²² were eliminated (Methods, Fig. 1 and Extended Data Table 1).

The best-scoring molecules from each of the top 10,000 clusters were inspected for engagement with residues that recognize ligands in the MT₁ crystal structure^{13,14} and for new polar partners in the MT₁ site. In the docked complexes, these included hydrogen bonds with

¹Department of Pharmaceutical Chemistry, University of California San Francisco, San Francisco, CA, USA. ²Department of Pharmacology, School of Medicine, University of North Carolina at Chapel Hill, Chapel Hill, NC, USA. ³Department of Pharmacology and Toxicology, Jacobs School of Medicine and Biomedical Sciences, University at Buffalo (SUNY), The State University of New York, Buffalo, NY, USA. ⁴Enamine Ltd, Kiev, Ukraine. ⁵National Taras Shevchenko University of Kyiv, Kiev, Ukraine. ⁶Chemspace, Monmouth Junction, NJ, USA. ⁷Bridge Institute, USC Michelson Center for Convergent Biosciences, University of Southern California, Los Angeles, CA, USA. ⁸Department of Chemistry, University of Southern California, Los Angeles, CA, USA. ⁹Present address: Department of Cell Biology, Neurobiology and Anatomy, Medical College of Wisconsin, Milwaukee, WI, USA. ¹⁰Present address: Designer Drug Research Unit, National Institute on Drug Abuse Intramural Research Program, Baltimore, MD, USA. ¹¹These authors contributed equally: Reed M. Stein, Hye Jin Kang, John D. McCorvy, Grant C. Glatfelter. ¹²These authors jointly supervised this work: Brian K. Shoichet, Bryan L. Roth, Margarita L. Dubocovich. ✉e-mail: bshoichet@gmail.com; bryan_roth@med.unc.edu; mdubo@buffalo.edu

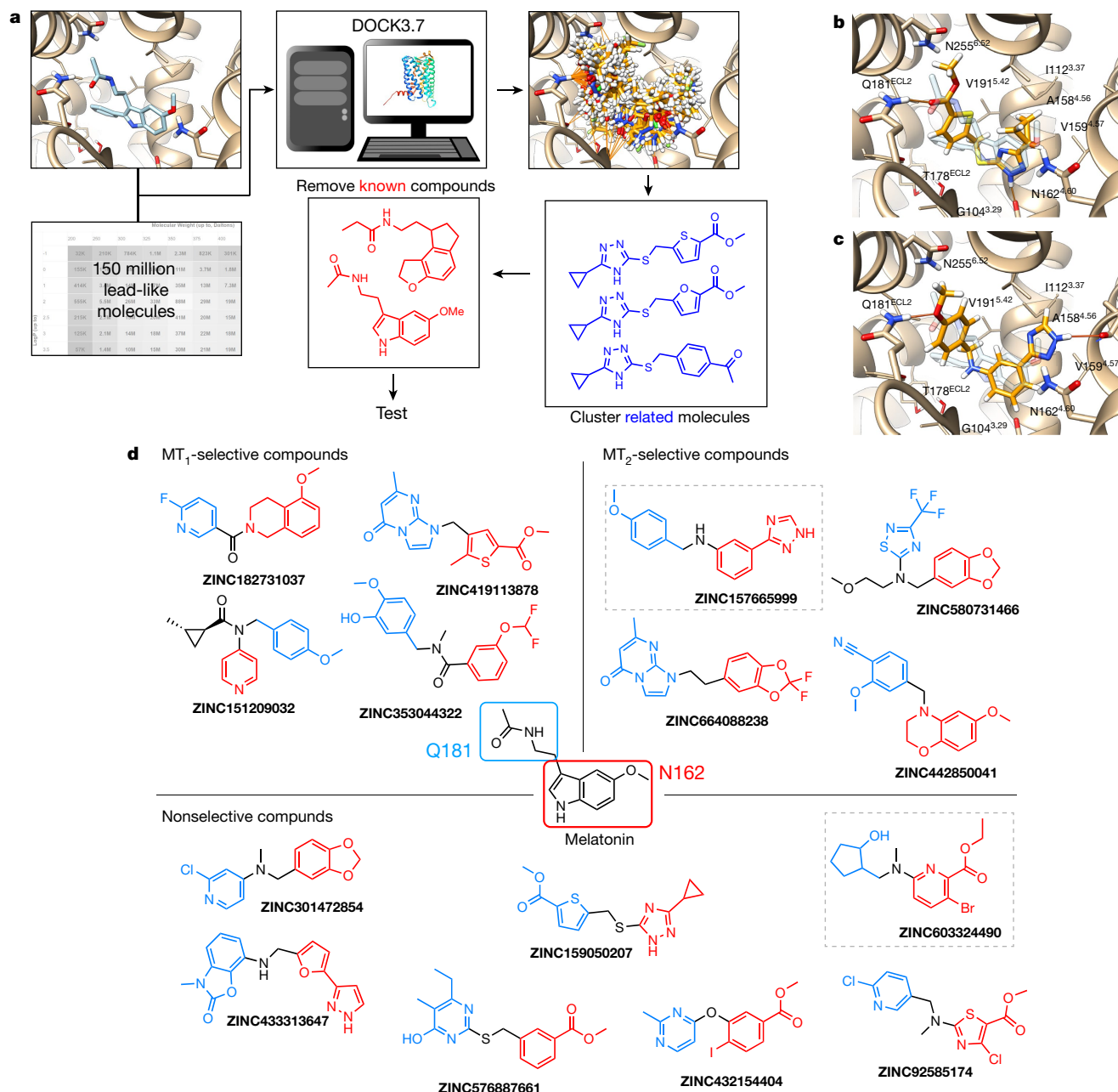


Fig. 1 | Large library docking finds novel, potent melatonin receptor ligands.

a, Docking for new melatonin receptor chemotypes from the make-on-demand library. **b**, Docked pose of **ZINC159050207**, an hMT₁/hMT₂ non-selective agonist with low nanomolar activity. **c**, Docked pose of **ZINC157665999**, an MT₂-selective inverse agonist. In **b** and **c**, the crystallographic geometry of

Q181^{ECL2}, N162^{4.60}, T178^{ECL2} and N255^{6.52}, and hydrogen bonds with the backbone atoms of A158^{4.56}, G104^{3.29} and F179^{ECL2}. Conformationally strained molecules and those with unsatisfied hydrogen-bond donors were deprioritized²³. Within the best-scoring clusters, all members were inspected and the one that best fitted these criteria was prioritized. Ultimately, 40 molecules with ranks ranging from 16 to 246,721, or the top 0.00001% to top 0.1% of the more than 150 million docked molecules, were selected for de novo synthesis and testing. Of the 38 molecules that were successfully synthesized (a 95% fulfilment rate), 15 had activity at either or both of the human MT₁ and MT₂ receptors in functional assays (Fig. 1 and Extended Data Table 1), a hit rate of 39% (calculated as the number of active compounds/number of physically tested compounds).

2-phenylmelatonin is shown in transparent blue, for context. **d**, The initial 15 docking actives are shown, highlighting groups that correspond to melatonin's acetamide side chain (blue) and its 5-methoxy-indole (red) in their docked poses and receptor interactions. Boxed molecules are inverse agonists.

Discovery of chemotypes with distinct efficacies

These active molecules included both agonists and inverse agonists, consistent with the emphasis on chemotype novelty (Fig. 1 and Extended Data Table 1). This novelty is supported quantitatively by their low topological similarity to known melatonin receptor ligands²⁴, and visually by comparison of the new ligands to their closest analogues among the known compounds (Extended Data Table 1). The different chemotypes often engaged the same residues that recognize 2-phenylmelatonin in the crystal structures. Examples include the hydrogen-bond interactions with N162^{4.60} made by the methoxy group of 2-phenylmelatonin that, in the docked models, were made by esters (**ZINC92585174**), pyridines (**ZINC151209032**) and benzodioxoles (**ZINC301472854**).

Similarly, whereas 2-phenylmelatonin stacks an indole with F179^{ECL2}, the docked ligands stack benzoxazines (**ZINC482850041**), thiophenes (**ZINC419113878**) and furans (**ZINC433313647**). Whereas 2-phenylmelatonin forms hydrogen bonds with Q181^{ECL2} through its acetamide, the docked ligands use esters or pyridines (Fig. 1). The new ligands also dock to interact with new residues, including hydrogen bonds with T178^{ECL2}, N255^{6.52}, A158^{4.56}, G104^{3.29} and F179^{ECL2} (Fig. 1b, c and Extended Data Fig. 3a–d).

Consistent with docking against an agonist-bound MT₁ structure, four of the ligands were MT₁-selective agonists (Extended Data Fig. 1a, b), with half-maximum effective concentration (EC₅₀) values in the 2–6 μM range, and without detectable MT₂ activity at concentrations of up to 30 μM: **ZINC419113878**, **ZINC151209032**, **ZINC353044322** and **ZINC182731037**. Notably, **ZINC159050207**—although it was not selective between the receptor types—is a 1 nM MT₁ agonist and is one of the most-potent molecules found directly from a docking screen^{25–30} (Fig. 1b, Extended Data Table 1 and Extended Data Fig. 1c, d). Admittedly, many ligands were just as active at the MT₂ receptor or were even selective for it (Extended Data Table 1 and Extended Data Fig. 1). Thus, although the initial docking against the MT₁ structure found new, potent chemotypes, and some of these were type-selective, they were just as likely to prefer the MT₂ type as the MT₁ type. This attests to both the strengths and weaknesses of chemotype novelty as a strategy for compound prioritization, and the need for further optimization.

We sought to improve 12 of these chemotype families, selecting analogues from the make-on-demand library. Several thousand such molecules were docked into the MT₁ site (see Methods and Extended Data Table 2). Of the 131 synthesized and tested, 94 analogues had activity at either or both the MT₁ or MT₂ melatonin receptors at concentrations of ≤10 μM (Extended Data Table 2, Extended Data Fig. 2 and Supplementary Table 1); of the 12 chemotype families, 5 showed improved potency. While this structure-based analogue-finding method could often find more-potent ligands, the efficacy, selectivity and bias of these compounds were sensitive to small structural changes (Extended Data Fig. 3).

We were particularly interested in type-selective ligands with in vivo efficacy, as these are unreported in the field. We investigated two MT₁-selective inverse agonists, **ZINC555417447** and **ZINC157673384**, and a selective MT₂ agonist, **ZINC128734226** (from here on referred to as **UCSF7447**, **UCSF3384** and **UCSF4226**, respectively), for their affinities (Fig. 2 and Supplementary Data 3, 4), in vitro signalling, pharmacokinetics (Extended Data Table 3), selectivity to mouse as well as the human melatonin receptors (Fig. 2 and Supplementary Data 3, 4), and for their efficacies in mouse models of circadian behaviour (Fig. 3 and Extended Data Figs. 4, 5, 7). As expected, **UCSF7447** and **UCSF3384** competed for 2-[¹²⁵I]iodomelatonin binding with higher affinity for the human MT₁ receptors. Inhibition constant (*K_i*) values in the absence of GTP—304 nM and 938 nM for **UCSF7447** and **UCSF3384**, respectively—were improved by uncoupling the G protein from the receptor by addition of GTP, with *K_i* values improving to 7.5 nM and 63 nM, respectively, supporting their status as inverse agonists (Fig. 2a, b, Extended Data Fig. 6 and Supplementary Data 3). Both **UCSF7447** and **UCSF3384** increased the basal levels of cAMP—also as expected for inverse agonists—with EC₅₀ values of 41 nM and 21 nM for human MT₁, selectivity for human MT₁ over human MT₂ of 53- and 31-fold, and inverse-agonist efficacies of 62% and 47% to human MT₁, respectively (Fig. 2c, d and Extended Data Fig. 6). The third molecule, **UCSF4226** was a human MT₂-selective agonist with an MT₂ over MT₁ selectivity of 54-fold in 2-[¹²⁵I]iodomelatonin binding assays and a selectivity of 91-fold in bioluminescence resonance energy transfer (BRET) assays; in isoproterenol-stimulated cAMP inhibition assays, the agonist had an EC₅₀ of 7.1 nM at human MT₂, a value closely matched by an EC₅₀ of 6.3 nM in BRET assays (Supplementary Data 4). After intravenous administration in mice, the three molecules were permeable in the central nervous system, with brain:plasma ratios ranging from 1.4 to 3.0. Plasma half-lives ranged from 0.27 to 0.32 h

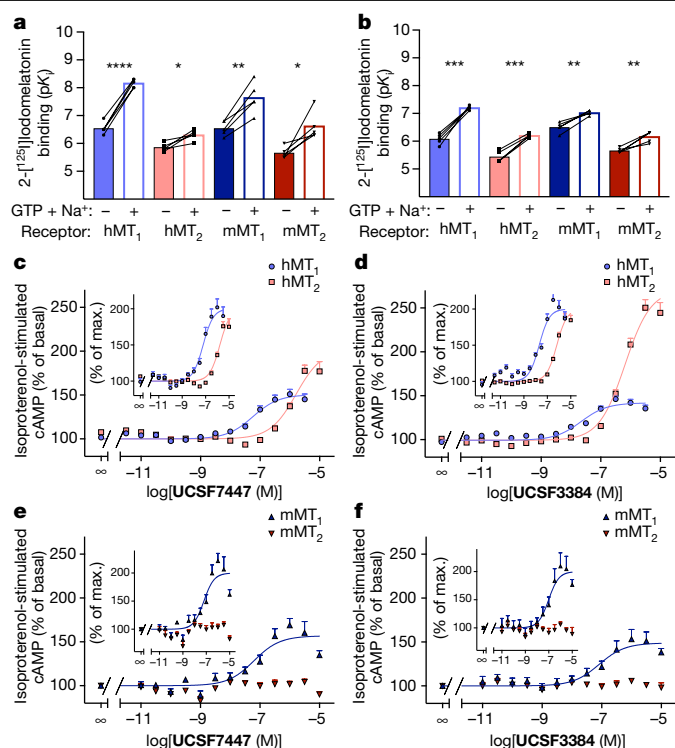


Fig. 2 | Affinity, efficacy and potency of MT₁-selective inverse agonists on human and mouse MT₁ and MT₂ receptors. **a, b**, Affinity (p*K_i*) of the inverse agonists **UCSF7447** (**a**) and **UCSF3384** (**b**) compared with 2-[¹²⁵I]iodomelatonin for human MT₁ (hMT₁), human MT₂ (hMT₂), mouse MT₁ (mMT₁) and mouse MT₂ (mMT₂) receptors stably expressed in CHO cells. Competitive binding was measured in the absence or presence of 100 μM GTP, 1 mM Na₂EDTA and 150 mM NaCl. GTP uncouples G proteins from melatonin receptors, thus promoting the inactive conformations of the receptors⁴⁶ and leading to a higher affinity of the receptors for inverse agonists. Therefore, the lighter-coloured bars show higher binding affinities for the drugs compared with the paired darker-coloured bars. Connected symbols represent the p*K_i* values of individual determinations run in parallel. *K_i* values were derived from competition binding curves (Supplementary Data 3). Bars represent the mean of five independent determinations. Statistical significance between p*K_i* averages was calculated by two-tailed paired Student's *t*-test (*t*, d.f. and *P* values are described in the 'Data analysis' Methods section, and Supplementary Table 5). **P* < 0.05; ***P* < 0.01; ****P* < 0.001; *****P* < 0.0001 compared with the corresponding p*K_i* averages values derived in the absence of GTP. **c–f**, Concentration–response curves of human and mouse MT₁ and MT₂ receptors that were transiently expressed in HEK293T cells. Analysis of isoproterenol-stimulated cAMP production combined with **UCSF7447** or **UCSF3384** treatment. Data for **UCSF7447** and **UCSF3384** were normalized to the isoproterenol-stimulated basal activity. Insets, data normalized to the maximum effect of **UCSF7447** or **UCSF3384**. **c**, Human MT₁ and MT₂ receptors treated with **UCSF7447**. hMT₁: pEC₅₀ = 7.39 ± 0.10, *E*_{max} = −62 ± 13%, *n* = 8; hMT₂: pEC₅₀ = 5.66 ± 0.10, *E*_{max} = −84 ± 9%, *n* = 8; hMT₂/hMT₁: EC₅₀ = 53. **d**, Human MT₁ and MT₂ receptors treated with **UCSF3384**. hMT₁: pEC₅₀ = 7.68 ± 0.09, *E*_{max} = −47 ± 12%, *n* = 13; hMT₂: pEC₅₀ = 6.18 ± 0.04, *E*_{max} = −153 ± 14%, *n* = 12; hMT₂/hMT₁: EC₅₀ = 31. **e**, Mouse MT₁ and MT₂ receptors treated with **UCSF7447**. mMT₁: pEC₅₀ = 7.20 ± 0.17, *E*_{max} = −56 ± 5%, *n* = 5; mMT₂: pEC₅₀, not determined, *E*_{max}, not determined, *n* = 5; mMT₂/mMT₁: EC₅₀ > 158. **f**, Mouse MT₁ and MT₂ receptors treated with **UCSF3384**. mMT₁: pEC₅₀ = 7.00 ± 0.22, *E*_{max} = −49 ± 3%, *n* = 5; mMT₂: pEC₅₀, not determined, *E*_{max}, not determined, *n* = 5; mMT₂/mMT₁: EC₅₀ > 100. Data represent mean ± s.e.m. of the indicated number (*n*) of biologically independent experiments run in triplicate.

(Extended Data Table 3), which is similar to melatonin². Against mouse MT₁ and MT₂ receptors in vitro, the selectivity of the inverse agonists **UCSF7447** and **UCSF3384** improved compared with the human receptors and were, respectively, more than 158 and 100 times more selective

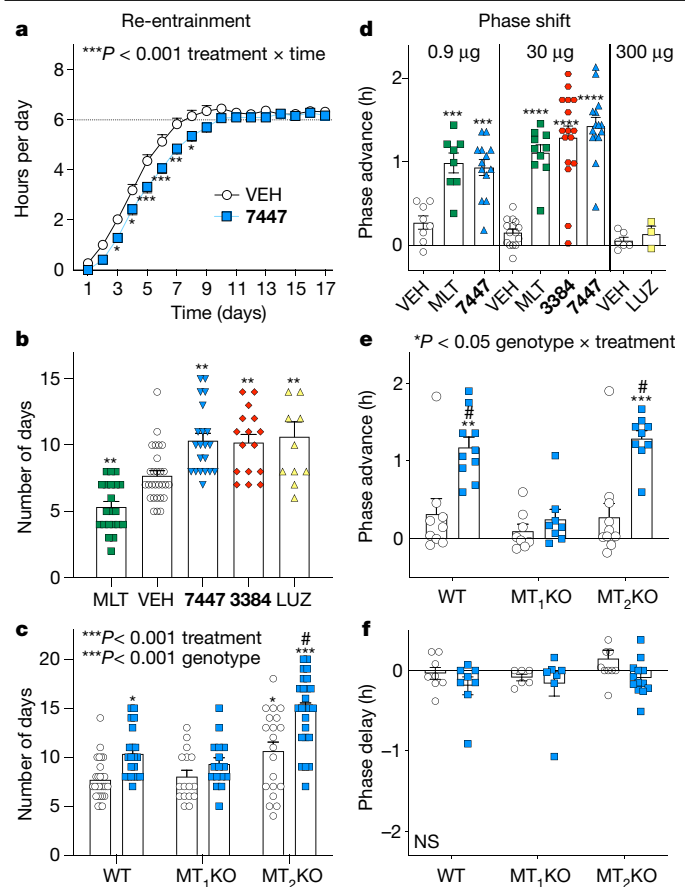


Fig. 3 | In vivo, MT₁-selective inverse agonists decelerate re-entrainment rate and induced a phase advance in circadian activity when administered at subjective dusk. **a, b,** In C3H/HeN wild-type (WT) mice, the inverse agonists **UCSF3384** and **UCSF7447** decelerate re-entrainment rate (**a**) and increase the number of days to re-entrainment after an advance of the dark onset by 6 h in the ‘eastbound jet-lag’ paradigm. **a,** Vehicle (VEH) versus **UCSF7447** (7447; 30 µg per mouse); mixed-effect two-way repeated-measures analysis of variance (ANOVA) (treatment × time interaction: $F_{16,735} = 3.39, P = 8.20 \times 10^{-6}$). **b,** Vehicle versus melatonin (MLT), **UCSF3384** (3384; 30 µg per mouse), **UCSF7447** (30 µg per mouse) or luzindole (LUZ; 300 µg per mouse); one-way ANOVA ($F_{4,92} = 16.97, P = 1.86 \times 10^{-10}$). **c,** The inverse agonist **UCSF7447** targets MT₁ receptors to increase the number of days to re-entrainment. Vehicle (white) versus **UCSF7447** (blue; 30 µg per mouse); two-way ANOVA (treatment: $F_{1,120} = 24.82, P = 2.14 \times 10^{-6}$; genotype: $F_{2,120} = 23.44, P = 2.55 \times 10^{-9}$). **d,** The inverse agonists **UCSF3384** and **UCSF7447** induce a phase advance in the onset of running wheel activity in constant dark at CT 10 (dusk), resembling the agonist melatonin. Left, vehicle versus melatonin or **UCSF7447** (0.9 µg per mouse); one-way ANOVA ($F_{2,26} = 13.60, P = 9.08 \times 10^{-5}$). Centre, vehicle versus melatonin, **UCSF3384** or **UCSF7447** (30 µg per mouse); one-way ANOVA ($F_{3,52} = 32.05, P = 7.15 \times 10^{-12}$). Right, vehicle versus luzindole (300 µg per mouse); two-tailed unpaired Student’s *t*-test ($t = 0.92, d.f. = 7, P = 0.39$). **e,** The phase advance of wheel activity onset by **UCSF7447** is mediated by the MT₁ receptor at CT 10 (dusk). Vehicle (white) versus **UCSF7447** (blue; 30 µg per mouse); two-way ANOVA (treatment × genotype interaction: $F_{2,49} = 4.46, P = 0.0166$). **f,** The inverse agonist **UCSF7447**, in contrast to melatonin, did not induce a phase delay in constant dark at CT 2 (dawn). Vehicle (white) versus **UCSF7447** (blue; 30 µg per mouse); two-way ANOVA (treatment × genotype interaction: $F_{2,49} = 0.384, P = 0.684$). In **f**, one value is not shown due to scale, but is included in the analysis (value = 0.91 h). Data are mean ± s.e.m. NS, not significant. * $P < 0.05$, ** $P < 0.01$, *** $P < 0.001$, **** $P < 0.0001$ compared with vehicle-treated wild-type mice. # $P < 0.001$; **** compared with vehicle-treated MT₂KO mice. Post-test analyses were carried out using Sidak’s (**a**), Tukey’s (**c, e, f**) or Dunnett’s (**b, d**; all $P < 0.05$) tests. Details for all statistical analyses and reporting of *n* values for each condition (depicted as scatter plots where appropriate) can be found in the Methods, ‘Statistics and reproducibility’ section and Supplementary Table 4. All mice were treated with different compound injections using subcutaneous injections.

for the mouse MT₁ receptor compared with the mouse MT₂ receptor at concentrations of up to 10µM for either compound (Fig. 2e, f and Supplementary Data 3). Conversely, whereas the agonist **UCSF4226** lost little activity against the mouse receptor, its selectivity for the mouse MT₂ receptor was much diminished (Supplementary Data 4). Accordingly, we moved forward to *in vivo* experiments in mice with the two selective MT₁ inverse agonists.

In vivo pharmacology reveals new MT₁ activities

We first examined the *in vivo* activity of the two MT₁-selective inverse agonists in a mouse model of re-entrainment. In this ‘east-bound jet-lag’ model, mice were subjected to an abrupt 6-h advance in the light–dark cycle and treated at the new onset of the dark for three consecutive days to assess re-entrainment rate. At 30 µg per mouse, the agonist melatonin accelerates re-entrainment to the new cycle, consistent with its use in the treatment of east-bound jet-lag in humans (Fig. 3b and Extended Data Fig 4b). Conversely, the prototypical non-selective antagonist/inverse agonist luzindole (administered at 300 µg per mouse) decelerates re-entrainment, measured as the number of days to adapt to the new dark onset (Fig. 3b and Extended Data Fig 4e), as expected for an inverse agonist^{31–33}. The selective MT₁ inverse agonists **UCSF7447** and **UCSF3384**, at a dose of 30 µg per mouse (about 1 mg kg⁻¹), also decelerated re-entrainment (Fig. 3a, b and Extended Data Fig. 4c, d, l), phenocopying luzindole (encouragingly, at a tenfold lower dose).

Superficially, the shared effect of decelerating re-entrainment by **UCSF7447**, **UCSF3384** (Fig. 3a, b and Extended Data Fig. 4c, d, l) and luzindole^{31,33} might seem expected, as all of the compounds share the same function as melatonin receptor antagonists/inverse agonists. However, luzindole is MT₁/MT₂ non-selective, in contrast to **UCSF7447** and **UCSF3384**. The phenocopying by the compounds of luzindole suggests that deceleration of re-entrainment by all three molecules—slowing jet-lag accommodation—is mediated through the MT₁ receptor alone. Supporting this, the effect of **UCSF7447** was eliminated in MT₁-knockout (MT₁KO) mice (Fig. 3c and Extended Data Fig. 4h, i, m), but not in MT₂-knockout (MT₂KO) mice, in which its effect was actually increased, adding to the deceleration induced by deletion of the MT₂ receptor alone (Fig. 3c and Extended Data Fig 4j, k, n).

The effect of the MT₁-selective inverse agonists on the circadian phase was even more unexpected. Here, we measured their effects on circadian phase by monitoring the running wheel activity onset of free-running mice in constant darkness^{34–36} and administering the drugs to the mice at subjective dusk (circadian time 10, CT 10). Both inverse agonists induced a phase advance in the onset of the circadian wheel running rhythm, an effect that is characteristic of melatonin—the endogenous, non-selective agonist—and of non-selective agonist drugs such as ramelteon³⁷ and agomelatine^{9,38} (Fig. 3d and Extended Data Fig. 5b–d, g, h). Whereas MT₁-selective inverse agonists have few if any precedents *in vivo*, we would have ordinarily expected the opposite effect of the agonist^{39,40}—that is, delaying rather than advancing the circadian phase. Instead, **UCSF7447** advanced the onset of activity by approximately 1 h at 0.9 µg per mouse (about 0.03 mg kg⁻¹), an effect similar to that of melatonin at its half-maximal effective dose (0.72 µg per mouse)³⁴ (Fig. 3d and Extended Data Fig. 5g, h). At a higher dose (30 µg per mouse, about 1 mg kg⁻¹), both **UCSF7447** and **UCSF3384** advanced the onset of running wheel activity with an amplitude similar to melatonin³⁴ at this circadian time (Fig. 3d and Extended Data Fig. 5b–d). Notably, whereas melatonin and ramelteon advance the phase when given at dusk (CT 10), and delay the phase when given at dawn (CT 2)^{35–37,41}, **UCSF7447** did not affect the circadian phase at dawn (Fig. 3f and Extended Data Fig 5r–w) and was only effective at dusk (Extended Data Fig. 7a–c).

The phenocopying effect of the non-selective agonist melatonin by the MT₁-selective inverse agonists in shifting circadian phase motivated

us to investigate the mechanism of action and the role of off-target effects. Accordingly, both molecules, as well as the human MT₂-selective agonist **UCSF4226**, were tested against a panel of common off-target receptors (Supplementary Data 1). In radioligand competition assays, no activity was seen up to a concentration of 10 μM for the new ligands. Against a panel of 318 G-protein-coupled receptors (GPCRs), activity was observed for only seven receptors when screened at a single concentration, activity against none of these seven receptors was replicated in full concentration–response assays (Supplementary Data 2).

Consistent with activity mediated by the MT₁ receptor, the advance in the onset of running wheel activity at dusk (CT 10) by **UCSF7447** was eliminated in MT₁KO mice but not in MT₂KO mice (Fig. 3e and Extended Data Fig. 5l–q). These observations suggest that the MT₁-selective inverse agonists **UCSF7447** and **UCSF3384** are not only potent, with effects on phase shift for **UCSF7447** at 0.9 μg per mouse (about 0.03 mg kg⁻¹) (Fig. 3d) and efficacies that resemble the long-established reagent luzindole in the jet-lag model at tenfold lower doses, but also that their unexpected activity in the circadian phase paradigm is mediated by the MT₁ receptor. We note that the lack of precedence for this behaviour reflects a lack of MT₁-selective inverse agonists to investigate this effect, something that is addressed by this study.

Discussion

We discovered, in a large library docking screen, multiple, previously undescribed chemotypes for melatonin receptors (Fig. 1) that have new signalling mechanisms and pharmacology. Three features of this study are worth emphasizing. First, docking a library of more than 150 million diverse, make-on-demand molecules found ligands that are topologically unrelated to known melatonin receptor ligands, with picomolar and nanomolar activity on the melatonin receptors. Second, the chemical novelty of these molecules translated functionally, conferring melatonin-receptor-type selectivity. Whereas the deceleration of re-entrainment (jet-lag model) by these inverse agonists resembled that of the classic non-selective antagonist/inverse agonist luzindole, their high selectivity for the MT₁ receptor, and the chemical–genetic epistasis in the MT₁KO mouse, convincingly implicates the MT₁ receptor in this response. Unexpectedly, the inverse agonists conferred an agonist-like effect in circadian phase-shift experiments when administered at dusk, perhaps suggesting previously unknown signalling control for the MT₁ receptor in the suprachiasmatic nucleus of the hypothalamus, which has known time-of-day-dependent receptor-mediated signalling pathways⁴². Third, these are, to our knowledge, the first MT₁-selective inverse agonists that are active in vivo, with efficacy at doses as low as 0.9 μg per mouse in the circadian phase shift paradigm. Their efficacy in modulating time-dependent circadian entrainment supports their potential as lead molecules for the design of therapeutics for conditions and diseases that are affected by alterations in the circadian phase^{5–7,43}.

Certain caveats should be noted. Although we sought MT₁-selective ligands, we found ligands for both melatonin receptor types, reflecting their conserved orthosteric sites. Indeed, rather than adopting a structure-based strategy for type selectivity, we simply focused on chemical novelty among the high-ranking docked molecules^{15,17}. Although the 39% docking hit rate was high, and the hits were potent, this probably reflects a site that is unusually well-suited to ligand binding: it is small, solvent-occluded and largely hydrophobic. These high hit rates and potencies may not always translate to other targets^{44,45}.

The key observations of this work should nevertheless be clear. From a structure-based screen of a diverse, 150 million compound virtual library sprang 15 new chemical scaffolds, topologically unrelated to known melatonin receptor ligands, synthesized de novo for this project. From their chemical novelty emerged previously undescribed activities, including inverse agonists and ligands with melatonin-receptor-type selectivity. The potency, brain exposure and selectivity of these ligands enable the disentanglement of the physiological role of the

MT₁ receptor. Accordingly, we are making the MT₁-selective inverse agonist **UCSF7447**, and the human MT₂ selective agonist **UCSF4226**, openly available to the community as probe pairs together with a close analogue that has no measurable activity on the melatonin receptors (Extended Data Table 4). We note that only a small fraction of even the highest-ranking chemotypes from the docking screen were tested here; it is likely that hundreds-of-thousands of melatonin receptor ligands, representing tens-of-thousands of new chemotypes¹⁵, remain to be discovered from the make-on-demand library, which continues to grow (<http://zinc15.docking.org>). This study suggests that not only potent ligands may be revealed by docking such a library, but also that the new chemotypes explored can illuminate new in vivo pharmacology.

Online content

Any methods, additional references, Nature Research reporting summaries, source data, extended data, supplementary information, acknowledgements, peer review information; details of author contributions and competing interests; and statements of data and code availability are available at <https://doi.org/10.1038/s41586-020-2027-0>.

1. Zisapel, N. New perspectives on the role of melatonin in human sleep, circadian rhythms and their regulation. *Br. J. Pharmacol.* **175**, 3190–3199 (2018).
2. Dubocovich, M. L. et al. International Union of Basic and Clinical Pharmacology. LXXV. Nomenclature, classification, and pharmacology of G protein-coupled melatonin receptors. *Pharmacol. Rev.* **62**, 343–380 (2010).
3. Liu, J. et al. MT1 and MT2 melatonin receptors: a therapeutic perspective. *Annu. Rev. Pharmacol. Toxicol.* **56**, 361–383 (2016).
4. Dubocovich, M. L. Melatonin receptors: role on sleep and circadian rhythm regulation. *Sleep Med.* **8**, 34–42 (2007).
5. Munday, K., Benloucif, S., Harsanyi, K., Dubocovich, M. L. & Zee, P. C. Phase-dependent treatment of delayed sleep phase syndrome with melatonin. *Sleep* **28**, 1271–1278 (2005).
6. Rajaratnam, S. M. et al. Melatonin agonist tasimelteon (VEC-162) for transient insomnia after sleep-time shift: two randomised controlled multicentre trials. *Lancet* **373**, 482–491 (2009).
7. Lewy, A. J. et al. The phase shift hypothesis for the circadian component of winter depression. *Dialogues Clin. Neurosci.* **9**, 291–300 (2007).
8. Jockers, R. et al. Update on melatonin receptors: IUPHAR Review 20. *Br. J. Pharmacol.* **173**, 2702–2725 (2016).
9. de Bodinat, C. et al. Agomelatine, the first melatonergic antidepressant: discovery, characterization and development. *Nat. Rev. Drug Discov.* **9**, 628–642 (2010).
10. Descamps-François, C. et al. Design and synthesis of naphthalenic dimers as selective MT₁ melatonergic ligands. *J. Med. Chem.* **46**, 1127–1129 (2003).
11. Spadoni, G. et al. Bivalent ligand approach on N-2-[(3-methoxyphenyl)methylamino] ethylacetamide: synthesis, binding affinity and intrinsic activity for MT₁ and MT₂ melatonin receptors. *Bioorg. Med. Chem.* **19**, 4910–4916 (2011).
12. Zlotos, D. P., Riad, N. M., Osman, M. B., Dodda, B. R. & Witt-Enderby, P. A. Novel difluoroacetamide analogues of agomelatine and melatonin: probing the melatonin receptors for MT₁ selectivity. *MedChemComm* **6**, 1340–1344 (2015).
13. Stauch, B. et al. Structural basis of ligand recognition at the human MT₁ melatonin receptor. *Nature* **569**, 284–288 (2019).
14. Johansson, L. C. et al. XFEL structures of the human MT₂ melatonin receptor reveal the basis of subtype selectivity. *Nature* **569**, 289–292 (2019).
15. Lyu, J. et al. Ultra-large library docking for discovering new chemotypes. *Nature* **566**, 224–229 (2019).
16. Weiss, D. R. et al. Selectivity challenges in docking screens for GPCR targets and antitargets. *J. Med. Chem.* **61**, 6830–6845 (2018).
17. Manglik, A. et al. Structure-based discovery of opioid analgesics with reduced side effects. *Nature* **537**, 185–190 (2016).
18. Huang, X. P. et al. Allosteric ligands for the pharmacologically dark receptors GPR68 and GPR65. *Nature* **527**, 477–483 (2015).
19. Lansu, K. et al. In silico design of novel probes for the atypical opioid receptor MRGPRX2. *Nat. Chem. Biol.* **13**, 529–536 (2017).
20. Sterling, T. & Irwin, J. J. ZINC 15—ligand discovery for everyone. *J. Chem. Inf. Model.* **55**, 2324–2337 (2015).
21. Coleman, R. G., Carchia, M., Sterling, T., Irwin, J. J. & Shoichet, B. K. Ligand pose and orientational sampling in molecular docking. *PLoS ONE* **8**, e75992 (2013).
22. Bento, A. P. et al. The ChEMBL bioactivity database: an update. *Nucleic Acids Res.* **42**, D1083–D1090 (2014).
23. Irwin, J. J. & Shoichet, B. K. Docking screens for novel ligands conferring new biology. *J. Med. Chem.* **59**, 4103–4120 (2016).
24. Muchmore, S. W. et al. Application of belief theory to similarity data fusion for use in analog searching and lead hopping. *J. Chem. Inf. Model.* **48**, 941–948 (2008).
25. Katritch, V. et al. Structure-based discovery of novel chemotypes for adenosine A_{2A} receptor antagonists. *J. Med. Chem.* **53**, 1799–1809 (2010).
26. de Graaf, C. et al. Crystal structure-based virtual screening for fragment-like ligands of the human histamine H₁ receptor. *J. Med. Chem.* **54**, 8195–8206 (2011).
27. Männel, B. et al. Structure-guided screening for functionally selective D₂ dopamine receptor ligands from a virtual chemical library. *ACS Chem. Biol.* **12**, 2652–2661 (2017).

28. Kiss, R. et al. Discovery of novel human histamine H4 receptor ligands by large-scale structure-based virtual screening. *J. Med. Chem.* **51**, 3145–3153 (2008).
29. Congreve, M. et al. Discovery of 1,2,4-triazine derivatives as adenosine A_{2A} antagonists using structure based drug design. *J. Med. Chem.* **55**, 1898–1903 (2012).
30. Langmead, C. J. et al. Identification of novel adenosine A_{2A} receptor antagonists by virtual screening. *J. Med. Chem.* **55**, 1904–1909 (2012).
31. Adamah-Biassi, E. B., Stepien, I., Hudson, R. L. & Dubocovich, M. L. Effects of the melatonin receptor antagonist (MT₂)/inverse agonist (MT₁) luzindole on re-entrainment of wheel running activity and spontaneous homecage behaviors in C3H/HeN Mice. *FASEB J.* **26**, 1042.5 (2012).
32. Dubocovich, M. L. Luzindole (N-0774): a novel melatonin receptor antagonist. *J. Pharmacol. Exp. Ther.* **246**, 902–910 (1988).
33. Browning, C., Beresford, I., Fraser, N. & Giles, H. Pharmacological characterization of human recombinant melatonin mt₁ and MT₂ receptors. *Br. J. Pharmacol.* **129**, 877–886 (2000).
34. Dubocovich, M. L., Yun, K., Al-Ghoul, W. M., Benloucif, S. & Masana, M. I. Selective MT₂ melatonin receptor antagonists block melatonin-mediated phase advances of circadian rhythms. *FASEB J.* **12**, 1211–1220 (1998).
35. Benloucif, S. & Dubocovich, M. L. Melatonin and light induce phase shifts of circadian activity rhythms in the C3H/HeN mouse. *J. Biol. Rhythms* **11**, 113–125 (1996).
36. Burgess, H. J., Revell, V. L., Molina, T. A. & Eastman, C. I. Human phase response curves to three days of daily melatonin: 0.5 mg versus 3.0 mg. *J. Clin. Endocrinol. Metab.* **95**, 3325–3331 (2010).
37. Rawashdeh, O., Hudson, R. L., Stepien, I. & Dubocovich, M. L. Circadian periods of sensitivity for ramelteon on the onset of running-wheel activity and the peak of suprachiasmatic nucleus neuronal firing rhythms in C3H/HeN mice. *Chronobiol. Int.* **28**, 31–38 (2011).
38. Van Reeth, O. et al. Comparative effects of a melatonin agonist on the circadian system in mice and Syrian hamsters. *Brain Res.* **762**, 185–194 (1997).
39. Erşahin, C., Masana, M. I. & Dubocovich, M. L. Constitutively active melatonin MT₁ receptors in male rat caudal arteries. *Eur. J. Pharmacol.* **439**, 171–172 (2002).
40. Soares, J. M. Jr, Masana, M. I., Erşahin, C. & Dubocovich, M. L. Functional melatonin receptors in rat ovaries at various stages of the estrous cycle. *J. Pharmacol. Exp. Ther.* **306**, 694–702 (2003).
41. Lewy, A. J. et al. The human phase response curve (PRC) to melatonin is about 12 hours out of phase with the PRC to light. *Chronobiol. Int.* **15**, 71–83 (1998).
42. Gillette, M. U. & Mitchell, J. W. Signaling in the suprachiasmatic nucleus: selectively responsive and integrative. *Cell Tissue Res.* **309**, 99–107 (2002).
43. Reid, K. J. et al. Familial advanced sleep phase syndrome. *Arch. Neurol.* **58**, 1089–1094 (2001).
44. Kufareva, I., Gustavsson, M., Zheng, Y., Stephens, B. S. & Handel, T. M. What do structures tell us about chemokine receptor function and antagonism? *Annu. Rev. Biophys.* **46**, 175–198 (2017).
45. Cooke, R. M., Brown, A. J., Marshall, F. H. & Mason, J. S. Structures of G protein-coupled receptors reveal new opportunities for drug discovery. *Drug Discov. Today* **20**, 1355–1364 (2015).
46. Lefkowitz, R. J., Mullikin, D. & Caron, M. G. Regulation of β -adrenergic receptors by guanyl-5'-yl imidodiphosphate and other purine nucleotides. *J. Biol. Chem.* **251**, 4686–4692 (1976).

Publisher's note Springer Nature remains neutral with regard to jurisdictional claims in published maps and institutional affiliations.

© The Author(s), under exclusive licence to Springer Nature Limited 2020

Methods

Molecular docking

The MT₁ receptor with nine thermostabilizing point mutations, as determined crystallographically¹³, was used in the docking calculations. To prepare the structure for docking, atoms of the co-crystallized ligand, 2-phenylmelatonin, were used to seed the matching sphere calculation in the orthosteric site; these spheres represent favourable positions for individual ligand atoms to dock; 45 spheres were used in total. DOCK3.7 orients flexibases of pre-calculated ligand conformations into the orthosteric site by overlaying atoms of each library molecule onto these matching spheres. The receptor structure was protonated by REDUCE⁴⁷ and assigned AMBER united atom charges⁴⁸. For residues N162^{4,60} and Q181^{ECL2}, the partial atomic charges of the side chain amide were increased without changing the net charge of the residue, as described previously⁴⁹. The volume of the low protein dielectric, which defines the boundary between solute and solvent in Poisson–Boltzmann electrostatic calculations, was extended out 1.9 Å from the protein surface using spheres calculated by SPHGEN. Scoring grids were pre-calculated using CHEMGRID for AMBER van der Waals potential, QNIFFT⁵⁰ for Poisson–Boltzmann-based electrostatic potentials, and SOLVMAP⁵¹ for ligand desolvation.

The resulting potential grids and ligand-matching parameters were evaluated for their ability to enrich known MT₁ ligands over property-matched decoys. Decoys share the same physical properties as known ligands but are topologically dissimilar and are therefore unlikely to bind to the receptors. We extracted 31 known MT₁ melatonin receptor ligands—both agonists and antagonists—from the IUPHAR database⁵² and 1,550 property-matched decoys were generated using the DUD-E pipeline. Docking success was judged based on the ability to enrich the known ligands over the decoys by docking rank, using adjusted logAUC values, as is widely done in the field. We also ensured that molecules with extreme physical properties were not enriched, as can happen when only counter-screening against property-matched decoys. In particular, we wanted to ensure that neutral molecules were enriched over charged ones. The docking parameters were also judged on how well they reproduced the expected binding modes of the known ligands as well as their ability to form hydrogen bonds with N162^{4,60} and Q181^{ECL2}.

The 'lead-like' subset of ZINC15 (<http://zinc15.docking.org>), characterized by favourable physical properties (for example, with calculated octanol-water partition coefficients (cLopP) ≤ 3.5 and with molecular mass ≤ 350 Da), was then docked against the MT₁ orthosteric site²¹, using DOCK3.7. This library contained more than 150 million molecules, most of which were make-on-demand compounds from the Enamine REAL set¹⁵. Of these, more than 135 million molecules successfully docked, with more than 36 million receiving a favourable score (< 0 kcal mol⁻¹). An average of 3,445 orientations was calculated for each, and for each orientation, an average of 485 conformations was sampled. A simplex minimizer was used for rigid-body minimization on the best-scored pose for each ligand. Overall, about 72 trillion complexes were sampled and scored. The calculation time was 45,020 core hours, or 1.25 calendar days on 1,500 cores.

To reduce the redundancy of the best-ranking docked molecules, the top 300,000 ranked molecules were clustered by ECFP4-based Tanimoto coefficient (Tc) of 0.5, and the best-scoring member was used to represent the cluster. The resulting 65,323 clusters were filtered for novelty by calculating the ECFP4-based Tanimoto coefficient against $> 1,100$ MT₁ and MT₂ receptor ligands from the ChEMBL23²² database. Molecules with Tanimoto coefficients of ≥ 0.38 to known MT₁/MT₂ ligands were not further pursued.

After filtering for novelty, the docked poses of the best-scoring members of each cluster were filtered by the proximity of their polar moieties to N162^{4,60} or Q181^{ECL2}, and manually inspected for favourable geometry and interactions. Of the best-scoring molecules prioritized in this way, all members of its cluster within the top 300,000 molecules

were also inspected, and sometimes one of these was chosen if they exhibited more favourable poses or chemical properties. Finally, 40 compounds were chosen for testing, 38 of which were successfully synthesized. To our knowledge, none of these compounds has been previously available and we are unaware of reports of them being previously synthesized.

Make-on-demand synthesis

Compounds were synthesized using 72,000 qualified in stock building blocks and 130 well-characterized, two-component reactions at Enamine. Previously, molecules have been synthesized in 3–4 weeks with an 85% fulfilment rate; in this project the delivery time was 6 weeks, but with a 95% fulfilment rate for the 40 molecules that were prioritized from the initial docking screen. Each reaction is tested for conditions including temperatures, completion time and mixing⁵³. Typically, compounds were made in parallel by combining reagents and solvents in a single vial in the appropriate conditions to allow the reaction to proceed to completion. The product-containing vial is filtered by centrifugation into a second vial to remove the precipitate and the solvent is evaporated under reduced pressure; the product is then purified by high-performance liquid chromatography. Identity and purity are assessed by liquid chromatography–mass spectrometry (LC–MS) and, as appropriate, ¹H NMR (Supplementary Table 2, Supplementary Data 7). All compounds were shipped with a purity of 90% or better, and the three main compounds **UCSF7447**, **UCSF3384** and **UCSF4226** were independently confirmed to be $\geq 95\%$ pure by LC–MS in secondary confirmation analyses at a second laboratory (Supplementary Data 5). Details regarding the synthesis and analyses of the compounds are provided in Supplementary Data 6, 7.

Structure-based ligand optimization

After experimental testing (see 'cAMP assay'), 12 of the 15 active ligands from docking were prioritized for optimization, representing a range of activities and type selectivity (Extended Data Table 2 and Supplementary Table 1). Several thousand analogues of these ligands—each bearing the same scaffold as the parent molecule and with a Tanimoto coefficient of < 0.38 to annotated melatonin receptor ligands—were selected from the ZINC database and docked to the MT₁ binding site, again using DOCK3.7. The resulting docked poses were manually evaluated for interactions with N162^{4,60} or Q181^{ECL2}, and 132 analogues were selected for de novo synthesis at Enamine, in two iterations. Of these, 131 were successfully synthesized, a $> 99\%$ fulfilment rate.

Cell culture

HEK293T cells were maintained with complete Dulbecco's modified Eagle's medium (DMEM), supplemented with 10% fetal bovine serum (FBS), 2 mM L-glutamine, 100 U ml⁻¹ penicillin G and 100 µg ml⁻¹ streptomycin. Cells were maintained at 37 °C in the presence of 5% CO₂.

Tango arrestin recruitment assay

MT₁ and MT₂ Tango constructs were designed and assays were performed as previously described⁵⁴. In brief, HTLA cells stably expressing TEV-protease-fused β -arrestin (provided by R. Axel) and a tTA-dependent luciferase reporter gene were transfected with the MT₁ or MT₂ Tango construct. The next day, transfected cells were seeded into poly-L-lysine-coated 384-well white clear-bottom cell-culture plates with DMEM containing 1% dialysed FBS at a density of 20,000 cells per well in 40 µl for another 6 h. The drug-containing solution was prepared in the same medium as used for cell plating at 5× final concentration and 10 µl per well was added for overnight incubation. The next day, medium and drug solutions were discarded and wells were loaded with 20 µl per well of Bright-Glo reagent (Promega). Plates were incubated for 20 min in the dark, after which luminescence was counted for the cell using a SpectraMax luminescence reader (Molecular Device). Data were analysed using GraphPad Prism 6.0 (GraphPad Software).

cAMP assay

MT₁ and MT₂ receptors were tested using split luciferase-based GloSensor cAMP biosensor technology (Promega). HEK293T cells were plated in 15-cm cell-culture dishes (at around 50% cell confluency) with DMEM supplemented with 10% dialysed FBS, 2 mM L-glutamine, 100 U ml⁻¹ penicillin G and 100 µg ml⁻¹ streptomycin for 4–6 h. Then, cells were co-transfected with 8 µg of constructs encoding either MT₁ or MT₂ (de-Tango-ized constructs) and 8 µg of Glosensor DNA. The next day, transfected cells were seeded into poly-L-lysine-coated 384-well white clear-bottom cell-culture plates with complete DMEM supplemented with 1% dialysed FBS at a density of 20,000 cells per well for another 24 h. The subsequent day, cell medium was discarded and wells were loaded with 20 µl of assay buffer (1× HBSS, 20 mM HEPES, pH 7.4, 0.1% BSA). To measure agonist activity of MT₁ or MT₂ receptor, 10 µl of test compound solution at 3× final concentration was added for 15 min followed by addition of 10 µl of luciferin/isoproterenol mixture (at a final concentration of 4 mM and 200 nM, respectively) for another 15 min for luminescence quantification. Then, plates were counted using a SpectraMax luminescence reader (Molecular Device). Data were analysed using GraphPad Prism 8.

Calculation of log(E_{\max}/EC_{50}) and quantification of ligand bias

The $\Delta\log(E_{\max}/EC_{50})$ was calculated with melatonin as a reference agonist for G protein and β -arrestin pathway, and the $\Delta\Delta\log(E_{\max}/EC_{50})$ was calculated between two pathways for each ligand⁵⁵, as were correspond-

ing bias plots⁵⁶. The bias factor is unitless and defined as $10^{\Delta\Delta\log(E_{\max}/EC_{50})}$.

GPCRome counterscreen

Screening of compounds in the PRESTO-Tango GPCRome was accomplished as previously described⁵⁴ with several modifications. First, HTLA cells were plated in DMEM with 10% FBS and 10 U ml⁻¹ penicillin-streptomycin. Next, the cells were transfected using an in-plate PEI method⁵⁷. PRESTO-Tango receptor DNAs were resuspended in OptiMEM and hybridized with PEI before dilution and distribution into 384-well plates and subsequent addition to cells. After overnight incubation, drugs were added to cells without replacement of the medium. The remaining steps of the PRESTO-Tango protocol were followed as previously described. For those six receptors for which activity was reduced to less than 0.5-fold of basal levels of relative luminescence units or for the one receptor for which basal signalling was increased greater than threefold of basal levels, assays were repeated as a full dose–response assay. Activity for none of the seven could be confirmed, and we discount the apparent activity seen in the single-point assay.

Inhibition screen

Binding assays were performed by the NIMH Psychoactive Drug Screening program as described previously⁵⁸. Detailed binding assay protocols are available at: <https://pdspdb.unc.edu/pdspWeb/content/UNC-CH%20Protocol%20Book.pdf>.

BRET recruitment assay

To measure the dissociation of labelled $G\alpha_{13}$ from the labelled $G\beta\gamma$ complex after the receptor stimulation, HEK293T cells were co-transfected in a 1:1:1:1 ratio of $G\alpha_{13}$ -RLuc, $G\beta3$, GFP2-G γ 9, and human MT₁ or MT₂ (de-Tango-ized constructs), respectively. After 24 h, transfected cells were plated in poly-L-lysine-coated 96-well white clear-bottom cell-culture plates with DMEM containing 1% dialysed FBS, 100 U ml⁻¹ penicillin G and 100 µg ml⁻¹ streptomycin at a density of 40,000 cells in 200 µl per well and incubated overnight. The following day, the medium was removed and cells were washed once with 100 µl of assay buffer (1× HBSS, 20 mM HEPES, pH 7.4, 0.1% BSA). Then 60 µl of assay buffer was loaded per well followed by addition of 10 µl of the RLuc substrate,

coelenterazine 400a (Nanolight), at 5 µM final concentration for 5 min. Drug stimulation was performed with the addition of 30 µl of 3× drug dilution of melatonin or UCSF4226 in assay buffer supplemented with 0.01% (w/v) ascorbic acid per well and incubated at room temperature for another 5 min. Both luminescence (400 nm) and fluorescent GFP2 emission (515 nm) were read for the plate for 1 s per well using Mithras LB940. The ratio of GFP2/RLuc was calculated per well and analysed using ‘log (agonist) vs. response’ in GraphPad Prism 8.

Radioligand binding

Reagents and ligands. 2-[¹²⁵I]iodomelatonin (SA: 2,200 Ci, 81.4 TBq mmol⁻¹) was purchased from Perkin Elmer. Guanosine 5'-triphosphate sodium salt hydrate (GTP), melatonin and all other chemicals and reagents were obtained from Sigma-Aldrich.

Compound preparation. For receptor binding studies, UCSF7447 was dissolved in 50% DMSO/50% ethanol as a 13 mM stock solution, diluted 1/10 in 100% ethanol then 1/10 again in 50% ethanol/50% Tris-HCl buffer, pH 7.4 25 °C. Both UCSF3384 and UCSF4226 were dissolved in 100% ethanol as 13 mM stock solutions and then diluted 1/10 in 50% ethanol/50% Tris-HCl buffer, pH 7.4. Further dilutions were done in the same Tris-HCl buffer.

2-[¹²⁵I]iodomelatonin competition binding. CHO cells stably expressing Flag-tagged recombinant human or mouse MT₁ or MT₂ melatonin receptors were grown in culture as monolayers in Ham's F12 medium supplemented with fetal calf serum (10%), penicillin (1%; 10,000 I.U. ml⁻¹)-streptomycin (5%; 10,000 µg ml⁻¹) in CO₂ at 37 °C as described. Cells were grown for 4 days to 90–95% confluence, then washed with PBS (potassium phosphate buffer, 10 mM, pH 7.4), detached with PBS containing 0.25 M sucrose and 1 mM EDTA, and pelleted by centrifugation (1,700g, 5 min) as described⁵⁹. Cell pellets were suspended and homogenized in control buffer (50 mM Tris-HCl, 10 mM MgCl₂; pH 7.4 at 25 °C) and washed twice by centrifugation (17,000g, 15 min) in control or inactive conformation buffer (50 mM Tris-HCl, 10 mM MgCl₂, 100 µM GTP, 1 mM EDTA-Na₂, 150 mM NaCl, pH 7.4 at 25 °C) as described⁵⁹. 2-[¹²⁵I]iodomelatonin binding affinity was determined on membranes from CHO cells expressing human MT₁ (9.6 ± 0.3 µg protein per assay; B_{\max} = 1,154 ± 38 fmol mg⁻¹ protein; n = 3), human MT₂ (15 ± 1 µg protein per assay; B_{\max} = 352 ± 19 fmol mg⁻¹ protein; n = 3), mouse MT₁ (6.0 ± 0.022 µg protein per assay; B_{\max} = 1,705 ± 337 fmol mg⁻¹ protein; n = 3) or mouse MT₂ (6.4 ± 0.7 µg protein per assay; B_{\max} = 725 ± 93 fmol mg⁻¹ protein; n = 3). Ligand competition (10 pM to 100 µM) for 2-[¹²⁵I]iodomelatonin (104 ± 2 pM, n = 30) binding was performed in control or inactive conformation buffer in a total volume of 0.26 ml as described⁵⁹. Assays were incubated for 1 h at 25 °C. Bound radioligand was separated from free by rapid vacuum filtration using glass microfibre filters (Whatman, Krackeler Scientific) saturated in 0.5% polyethylenimine solution. Total radioactivity bound to the filters was determined on a gamma counter⁵⁹.

Data analysis. K_i values were calculated from IC₅₀ values using GraphPad Prism 8.0 according to the Cheng–Prusoff equation⁶⁰: $K_i = IC_{50}/(1 + [L]/K_d)$ where L is the concentration of radioligand, K_d is the dissociation constant of 2-[¹²⁵I]iodomelatonin in control or inactive conformation buffer for the human MT₁ (control K_d = 116 pM; inactive K_d = 280 pM), human MT₂ (control K_d = 80 ± 13 pM; GTP K_d = 461 ± 159 pM) and mouse MT₁ (control K_d = 87 ± 6 pM; GTP K_d = 201 ± 67 pM) receptors (n = 3). Affinity shifts induced by G-protein uncoupling were measured by subtracting $pK_{i(\text{inactive})}$ from $pK_{i(\text{control})}$ (ΔpK_i) and normalization to the ΔpK_i of melatonin (CHO cells expressing human MT₁, 1.19; CHO cells expressing human MT₂, 0.41). Affinity shifts or lack thereof with G-protein uncoupling indicate apparent efficacy⁴⁶ as ligands are classified as agonists (ΔpK_i percentage of melatonin >20%), antagonists (ΔpK_i percentage of melatonin <20%, >-20%) or inverse agonists (ΔpK_i percentage of melatonin <-20%) accordingly. Individual data points were

excluded from cell-based analyses when meeting the exclusion criteria of the outliers Grubbs test. Data shown in Fig. 2a, b were analysed by two-tailed paired Student's *t*-test (Supplementary Table 5).

In vivo methods

Animals and housing. Male and female C3H/HeN wild-type, MT₁KO, and MT₂KO mice (average age, 6.28 months) used in this study were raised in our breeding colony at University at Buffalo. C3H/HeN mice homozygous for the MT₁ and MT₂ melatonin receptor gene deletion and their wild-type controls were generated from breeding pairs donated by S. M. Reppert (University of Massachusetts Medical School) and backcrossed with C3H/HeN mice (Harlan, now Envigo) for at least seven generations as described previously⁶¹. Genotype was confirmed using tail samples at the end of each experiment and was verified periodically during the tenure of the colony. The strains of mice in our breeding colony were re-derived periodically by backcrossing with wild-type mice to reduce genetic drift.

Mice were group-housed (3–5 per cage) with corn cob bedding in polycarbonate translucent cages (30 cm × 19 cm) and maintained in a 14/10 light–dark cycle (Zeitgeber time 0 (ZT 0) corresponds to lights on and ZT 14 to lights off) in temperature- and humidity-controlled rooms with ad libitum access to food and water in the Laboratory Animal Facility at the University at Buffalo. Light levels were 200–300 lx at the level of the cage. Treatments and animal care performed in the dark were carried out under a dim red safelight (15 W, Kodak 1A filter) with illuminance of less than 3 lx as described previously³⁵. All experimental procedures using mice were conducted in accordance with guidelines set forth by the National Institutes of Health and approved by the University at Buffalo Institutional Animal Care and Use Committee.

Circadian rhythm measurements. Circadian rhythm phase was determined for each mouse using the onset of running wheel activity defined as CT 12 (onset of wheel activity). Running wheel activity was measured continuously by magnetic microswitches that detect wheel revolutions using a computer equipped with ClockLab data-collection software (Actimetrics). All actigraphy data were visualized and analysed using ClockLab and MATLAB software. All mice were individually housed in cages (33 cm × 15 cm) equipped with running wheels in light-tight ventilated cabinets with controlled temperature and light–dark cycles (Phenome Technologies). Male and female mice were housed in separate cabinets for all experiments.

Phase shift. Changes in circadian phase induced by vehicle or drugs administered at various circadian times were assessed in wild-type, MT₁KO and MT₂KO male and female C3H/HeN mice (3–8 months of age) using methods and protocols that have been previously described^{34,35}. Following a period of 14 days in a light–dark cycle, mice were placed in constant dark beginning at ZT 12 (dark onset) (ZT 0, lights on). Mice were kept in constant dark (2–3 weeks) until a stable free-running phase of running wheel activity rhythm onset was established. Circadian times of treatment were predicted from best fit lines of running wheel activity onsets for running either before (7–14 days) and after (7–14 days) treatment. Treatment times were within a 2-h window at CT 2 (CT 1–3), CT 6 (CT 5–7) or CT 10 (CT 9–11). Mice were treated (0.1 ml per mouse, subcutaneously) with vehicle (30% ethanol saline, subcutaneously) or drugs (melatonin, UCSF3384 or UCSF7447, at 0.9 µg and 30 µg per mouse or luzindole at 300 µg per mouse in vehicle) for 3 consecutive days at the appropriate circadian time under dim red light. Vehicle or drug treatments were repeated for 3 consecutive days at the selected circadian time following the three-pulse treatment protocol described previously³⁵. Phase shifts were quantified using the best fit lines for onsets of activity during pre- and post-treatment periods. Differences are characterized as phase delays (pre-treatment ahead of post-treatment best fit line onset) or phase advances (post-treatment ahead of pre-treatment best fit line onset) of running wheel activity onset rhythms.

Re-entrainment experiments. Male and female C3H/HeN wild-type, MT₁KO and MT₂KO mice (3–6 months of age) were maintained under a 12:12 light–dark cycle for at least 2 weeks before experimental manipulations to enable stable entrainment to dark onset before advance of the light–dark cycle. Actigraphy data were recorded as described above and all experimental protocols were performed as described previously⁶². On the first day of treatment, the dark onset was advanced 6 h. This resulted in a short night. Mice were treated (0.1 ml per mouse, subcutaneously) with vehicle (30% ethanol/70% saline) or drugs (melatonin, UCSF3384 or UCSF7447 at 30 µg per mouse, or luzindole 300 µg per mouse, in vehicle) for three consecutive days 10–30 min before the new dark onset. After treatment, mice were given 14–20 days to re-entrain the onset of running wheel activity to the new dark onset. Using exported running wheel activity onsets from actograms, the number of onset hours advanced each day was determined by subtracting this value each day from the average onset of stably entrained running wheel activity for 3 days before treatment for each mouse. Furthermore, using the data from this calculation combined with visualization of actograms, the number of days to reach stable re-entrainment was determined for each mouse.

In vivo compound preparation. All compounds were administered in fixed doses of either 0.9 µg or 30 µg subcutaneously in a volume of 0.1 ml per mouse, which are equivalent to doses of 0.03 or 1 mg kg⁻¹ for a 30 g mouse, respectively. Vehicle was 30% ethanol/70% saline for all doses. Melatonin, UCSF7447 and UCSF3384 were prepared as stock solutions of 3 mg ml⁻¹ (100% ethanol) using sonication and vortexing to ensure that each drug was dissolved. Subsequently, stock solutions were diluted to 0.3 mg ml⁻¹ (30 µg per 0.1 ml injection) or 0.009 mg ml⁻¹ (0.9 µg per 0.1 ml injection) in vehicle. Luzindole was prepared similarly, except the starting stock solution was 30 mg ml⁻¹ in 100% ethanol and it was administered from a solution of 3 mg ml⁻¹ (300 µg per 0.1 ml injection) in vehicle. Treatment dilutions were prepared just before use under sonication with intermittent vortexing between steps and used within 5 min of preparation.

Biostatistics and reproducibility. All statistical analyses as described in further detail for each experiment were conducted using GraphPad Prism 8. For phase shift and re-entrainment experiments, we determined statistical power a priori (error probability, $\alpha = 0.05$) based on data for a known effect size for melatonin in these paradigms (G-power 3.0.10)^{34,62}. Individual actograms of wheel running activity were excluded from analysis based on the exclusion criteria described below, which was completed by at least two individuals who were blind to treatment before data analysis was started. For re-entrainment actograms exclusion criteria included: (1) low running, sporadic activity, substantial missing wheel activity data and/or lack of entrainment before treatment; (2) entrainment of running activity more than 1 h before or after the 'old' or 'new' dark onset; (3) re-entrainment to the new dark onset before administration of the third injection (entrainment to injection). For phase-shift actograms exclusion criteria included: (1) low running, sporadic activity, missing wheel activity data and/or lack of free running activity rhythms; (2) tau change >0.3 h; (3) at least two out of three injections occurred outside of the target predetermined time range for treatment (CT 1–3, 5–7, 10–12). All datasets were visualized for normality using QQ plots of predicted versus actual residuals. Actigraphy data were generated for visualization blind to treatment before the quantification and statistical analysis stages. Comparisons for Fig. 3a and Extended Data Fig. 4l, m, n were made by mixed-effect two-way repeated-measures ANOVA (treatment × time) with Sidak's post hoc test ($P < 0.05$). Number of days to re-entrainment was compared using one-way ANOVA or two-way ANOVA for Fig. 3b, c with a Dunnett's or Tukey's post hoc test ($P < 0.05$), respectively. Group comparisons for phase shift in Fig. 3d (left and centre) and Extended

Article

Data Fig. 7a–c were made by one-way ANOVA ($P < 0.05$) comparing hours shifted of circadian running wheel activity rhythm onsets (Fig. 3d (left), three groups: vehicle, melatonin and **UCSF7447**; Fig. 3d (centre), four groups: vehicle, melatonin, **UCSF7447** and **UCSF3384**; Extended Data Fig. 7a–c, four groups: vehicle, melatonin, **UCSF7447** and luzindole) accompanied by post hoc analyses using Dunnett's test to determine individual group differences compared with vehicle ($P < 0.05$). Comparisons in Fig. 3d (right) between vehicle and luzindole were made using a two-tailed unpaired Student's *t*-test ($P < 0.05$). Data in Fig. 3e, f were compared using a two-way ANOVA (3×2 : genotype \times treatment) with Tukey's post hoc analyses ($P < 0.05$). *P* values and values for statistical analyses are included in the figure legends or listed in Supplementary Table 4. Either the overall interaction or the main effects are reported and interpreted using two-way ANOVAs as appropriate for assumptions of each dataset. No sex differences in treatment effects were evident in any dataset when assessed by two-way ANOVA or three-way ANOVA where appropriate; therefore, data were pooled between male and female mice for the described analyses. The *n* values represent the number of individual mice per condition or independent biological replicates in each experiment. Each dataset represents 2–4 independent experiments. The *n* value for each in vivo experiment is listed below (*n* values with an asterisk indicate values for multiple comparisons ranging from 1 to 2 values less depending on the day of comparison due to missing onset data that are accounted for in statistical models as appropriate). See statistical parameters in Supplementary Table 4.

Figure 3a, vehicle ($n = 28$ mice*) versus **UCSF7447** ($n = 21$ mice*). Figure 3b, vehicle ($n = 28$) versus melatonin ($n = 21$), **UCSF7447** ($n = 21$), **UCSF3384** ($n = 16$) or luzindole ($n = 11$). Figure 3c, wild-type ($n = 28$ vehicle; $n = 21$ **UCSF7447**), MT_1 KO ($n = 16$ vehicle; $n = 16$ **UCSF7447**) and MT_2 KO ($n = 20$ vehicle; $n = 25$ **UCSF7447**). Figure 3d, left: vehicle ($n = 8$) versus melatonin ($n = 8$) or **UCSF7447** ($n = 13$); centre: vehicle ($n = 15$) versus melatonin ($n = 10$), **UCSF3384** ($n = 16$) or **UCSF7447** ($n = 15$); right: vehicle ($n = 6$) versus luzindole ($n = 3$). Figure 3e, wild-type ($n = 9$ vehicle; $n = 10$ **UCSF7447**), MT_1 KO ($n = 8$ vehicle; $n = 8$ **UCSF7447**) and MT_2 KO ($n = 11$ vehicle; $n = 9$ **UCSF7447**). Figure 3f, wild-type ($n = 8$ vehicle; $n = 8$ **UCSF7447**), MT_1 KO ($n = 6$ vehicle; $n = 7$ **UCSF7447**) and MT_2 -KO ($n = 10$ vehicle; $n = 13$ **UCSF7447**).

Extended Data Figure 4l, C3H/HeN wild-type: vehicle ($n = 28$ mice*) versus **UCSF3384** ($n = 16$ mice*). Extended Data Figure 4m, C3H/HeN MT_1 KO: vehicle ($n = 16$ mice*) versus **UCSF7447** ($n = 16$ mice*). Extended Data Figure 4n, C3H/HeN MT_2 KO: vehicle ($n = 21$ mice*) versus **UCSF7447** ($n = 25$ mice).

Extended Data Figure 7a, CT 2: vehicle ($n = 3$), melatonin ($n = 3$), luzindole ($n = 6$) and **UCSF7447** ($n = 3$). Extended Data Figure 7b, CT 6: vehicle ($n = 8$), melatonin ($n = 4$), luzindole ($n = 9$) and **UCSF7447** ($n = 9$). Extended Data Figure 7c, CT 10: vehicle ($n = 6$), melatonin ($n = 8$), luzindole ($n = 3$) and **UCSF7447** ($n = 4$)

Pharmacokinetics. Pharmacokinetic experiments were performed by Sai Life Sciences. Plasma pharmacokinetics and brain distribution for **UCSF7447**, **UCSF3384** and **UCSF4226** were investigated following a single intravenous dose of 2 mg kg^{-1} in 9 male C57BL/6 mice. Each compound was formulated in 5% *N*-methyl-pyrrolidone, 5% solutol HS-15 and 90% normal saline. Blood samples (approximately $60 \mu\text{l}$ from each of three mice) were collected under light isoflurane anaesthesia from the retro-orbital plexus at 0.08, 0.25, 0.5, 1, 2, 4, 8, 12 and 24 h. Immediately after collection, plasma was obtained by centrifugation and stored at -70°C until analysis. For blood collected at 0.5, 4 and 24 h, animals were euthanized with excess CO_2 asphyxiation and brain samples were collected and homogenized in ice-cold phosphate-buffered saline (pH 7.4). Total homogenate volume was three times the brain weight.

All samples were processed for analysis by protein precipitation using acetonitrile and analysed using a fit-for-purpose LC–MS/MS method (lower limit of quantification, 2.01 ng ml^{-1} for plasma and 6.03 ng g^{-1} for brain for **UCSF7447**, 5.01 ng ml^{-1} for plasma and 3.00 ng g^{-1} for

brain for **UCSF3384**, 1.01 ng ml^{-1} for plasma and 6.09 ng g^{-1} for brain for **UCSF4226**). The non-compartmental analysis module in Phoenix WinNonlin (v.7.0) was used to assess the pharmacokinetic parameters. The maximum concentration (C_{max}) and time to reach the maximum concentration (T_{max}) were measured. The areas under the concentration time curve (AUC_{last} and AUC_{int}) and elimination half-life were calculated by the linear trapezoidal rule. The terminal elimination rate constant, k_e , was determined by regression analysis of the linear terminal portion of the log plasma concentration–time curve. The terminal half-life ($T_{1/2}$) was estimated as $0.693/k_e$.

Reporting summary

Further information on research design is available in the Nature Research Reporting Summary linked to this paper.

Data availability

Probe pairs (two similar ligands with and without activity) of inverse agonists selective for MT_1 and agonists selective for hMT_2 are available by arrangement with Sigma (Extended Data Fig. 3). The identities of the compounds docked in this study are freely available from the ZINC database (<http://zinc15.docking.org>) and active compounds may be purchased from Enamine. Raw data are available for Fig. 1, Extended Data Tables 1, 2 and Extended Data Figs. 1, 2 in Supplementary Tables 1 (MT_1 and MT_2 affinities, MT_1 DOCK energies and ranks) and 2 (compound purity information). Bias information for Extended Data Fig. 3 is included in Supplementary Table 3. For Fig. 2, data from the GPCRome screens, concentration–response curves, and competition binding and LC–MS experiments are included in Supplementary Data 1–5 and synthesis routes and spectra of compounds in Supplementary Data 6, 7. Further data for Fig. 3 are included in Extended Data Figs. 4, 5, 7 and Supplementary Table 4. Raw data values and transformed data for in vitro cell-based assays as well as in vivo data for phase shift and re-entrainment are available for Figs. 2, 3 and Extended Data Figs. 4 (re-entrainment), 5 (phase shift), 6, 7a–c.

Code availability

DOCK3.7 is freely available for non-commercial research (<http://dock.compbio.ucsf.edu/DOCK3.7/>). A web-based version is freely available to all at <http://blaster.docking.org/>. The ultra-large library used here is freely available at <http://zinc15.docking.org/>.

- Word, J. M., Lovell, S. C., Richardson, J. S. & Richardson, D. C. Asparagine and glutamine: using hydrogen atom contacts in the choice of side-chain amide orientation. *J. Mol. Biol.* **285**, 1735–1747 (1999).
- Weiner, S. J. et al. A new force field for molecular mechanical simulation of nucleic acids and proteins. *J. Am. Chem. Soc.* **106**, 765–784 (1984).
- Carlsson, J. et al. Structure-based discovery of A_{2A} adenosine receptor ligands. *J. Med. Chem.* **53**, 3748–3755 (2010).
- Gallagher, K. & Sharp, K. Electrostatic contributions to heat capacity changes of DNA–ligand binding. *Biophys. J.* **75**, 769–776 (1998).
- Mysinger, M. M. & Shoichet, B. K. Rapid context-dependent ligand desolvation in molecular docking. *J. Chem. Inf. Model.* **50**, 1561–1573 (2010).
- Southan, C. et al. The IUPHAR/BPS guide to pharmacology in 2016: towards curated quantitative interactions between 1300 protein targets and 6000 ligands. *Nucleic Acids Res.* **44**, D1054–D1068 (2016).
- Tolmachev, A. et al. Expanding synthesizable space of disubstituted 1,2,4-oxadiazoles. *ACS Comb. Sci.* **18**, 616–624 (2016).
- Kroez, W. K. et al. PRESTO-Tango as an open-source resource for interrogation of the druggable human GPCRome. *Nat. Struct. Mol. Biol.* **22**, 362–369 (2015).
- Kenakin, T., Watson, C., Muniz-Medina, V., Christopoulos, A. & Novick, S. A simple method for quantifying functional selectivity and agonist bias. *ACS Chem. Neurosci.* **3**, 193–203 (2012).
- Kenakin, T. Biased receptor signaling in drug discovery. *Pharmacol. Rev.* **71**, 267–315 (2019).
- Longo, P. A., Kavran, J. M., Kim, M. S. & Leahy, D. J. Transient mammalian cell transfection with polyethylenimine (PEI). *Methods Enzymol.* **529**, 227–240 (2013).
- Besnard, J. et al. Automated design of ligands to polypharmacological profiles. *Nature* **492**, 215–220 (2012).
- Popovska-Gorevski, M., Dubocovich, M. L. & Rajnarayanan, R. V. Carbamate insecticides target human melatonin receptors. *Chem. Res. Toxicol.* **30**, 574–582 (2017).

60. Cheng, Y.-C. & Prusoff, W. H. Relationship between the inhibition constant (K_i) and the concentration of inhibitor which causes 50 per cent inhibition (I_{50}) of an enzymatic reaction. *Biochem. Pharmacol.* **22**, 3099–3108 (1973).
61. Sumaya, I. C., Masana, M. I. & Dubocovich, M. L. The antidepressant-like effect of the melatonin receptor ligand luzindole in mice during forced swimming requires expression of MT_2 but not MT_1 melatonin receptors. *J. Pineal Res.* **39**, 170–177 (2005).
62. Dubocovich, M. L., Hudson, R. L., Sumaya, I. C., Masana, M. I. & Manna, E. Effect of MT_1 melatonin receptor deletion on melatonin-mediated phase shift of circadian rhythms in the C57BL/6 mouse. *J. Pineal Res.* **39**, 113–120 (2005).

Acknowledgements This study was supported by US NIH awards U24DK1169195 (to B.L.R. and B.K.S.), R35GM122481 (to B.K.S.), the NIMH Psychoactive Drug Screening Contract (to B.L.R.), GM133836 (to J.J.I.), ESO23684 (to M.L.D.), UL1TR001412 and KL2TR001413 (to the University at Buffalo), a PhRMA Foundation Fellowship (73309 to A.J.J.), Jacobs School of Medicine and Biomedical Sciences unrestricted funds (to M.L.D.), R35GM127086 (to V.C.), EMBO ALTF 677-2014 (to B.S.), HFSP long-term fellowship LT000046/2014-L (to L.C.J.), a postdoctoral fellowship from the Swedish Research Council (to L.C.J.) and the National Science Foundation (NSF) BioXFEL Science and Technology Center 1231306 (to B.S. and V.C.). We thank G. Wilding from the Biostatistics, Epidemiology and Research Design (BERD) Core of the Clinical and Translational Science Institute at the University at Buffalo for statistical advice regarding analyses of in vivo data.

Author contributions B.K.S., B.L.R. and M.L.D. conceived the study. R.M.S. performed the docking and structure-based optimization. J.D.M. and H.J.K. performed the initial binding and functional assays and analyses, assisted by T.C. A.J.J. performed the 2-[125 I]iodomelatonin and GTP-perturbation assays. S.S. performed the profiling studies. G.C.G. performed the in vivo mouse pharmacology experiments and all animal husbandry. Y.S.M. and O.S. directed the compound synthesis, purification and characterization experiments. B.S., L.C.J., V.C., B.L.R., X.-P.H. and J.D.M. determined and validated the structures of the MT_1 and MT_2 receptor types, and made them available before publication. T.K. performed signalling bias calculations. J.J.I. created the ultra-large libraries. B.L.R. supervised the pharmacology studies; B.K.S. supervised the docking and compound optimization; M.L.D. supervised the binding studies and the in vivo circadian rhythm experiments in mice. M.L.D. G.C.G. designed all in vivo experiments. R.M.S., B.K.S., M.L.D., G.C.G., J.D.M., H.J.K. and B.L.R. wrote the paper with contributions from other authors.

Competing interests B.K.S. and J.J.I. are founders of a company, BlueDolphin LLC, that works in the area of molecular docking. All other authors declare no competing interests.

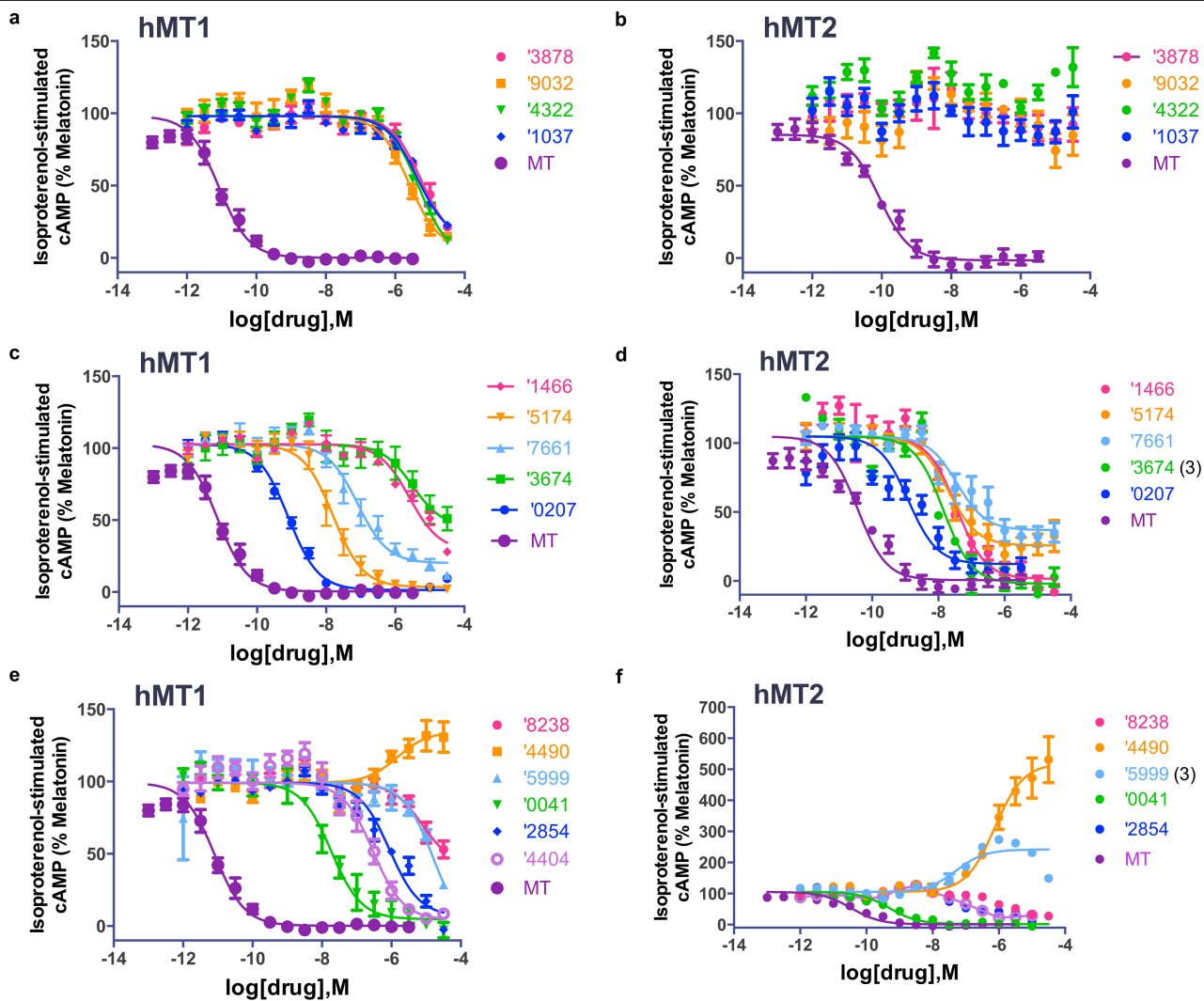
Additional information

Supplementary information is available for this paper at <https://doi.org/10.1038/s41586-020-2027-0>.

Correspondence and requests for materials should be addressed to B.K.S., B.L.R. or M.L.D.

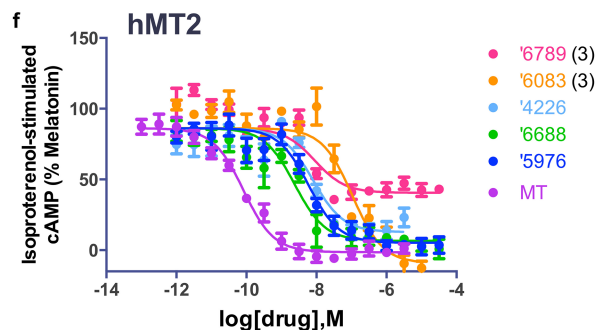
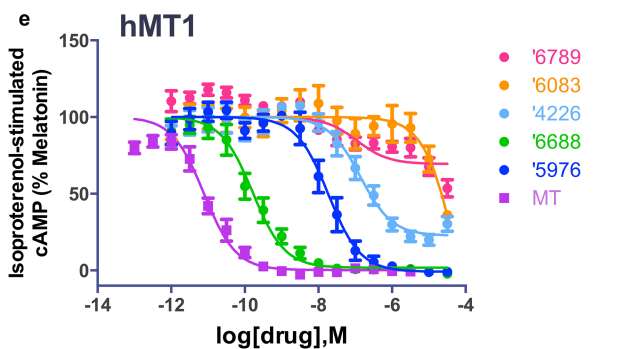
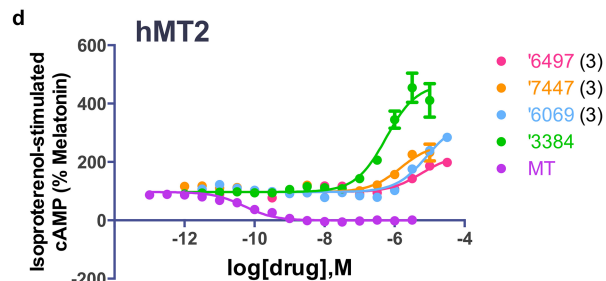
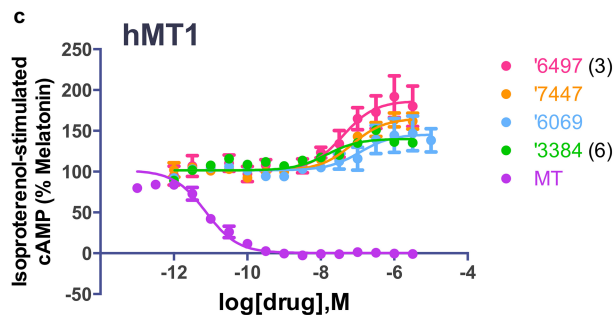
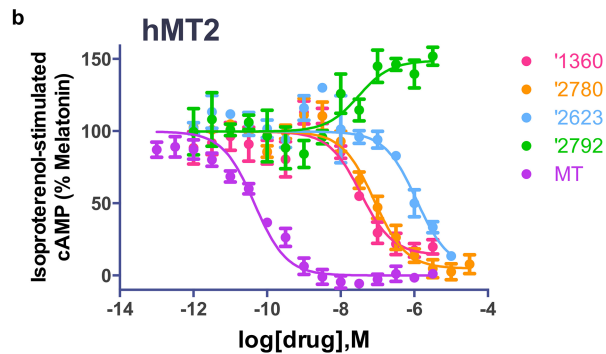
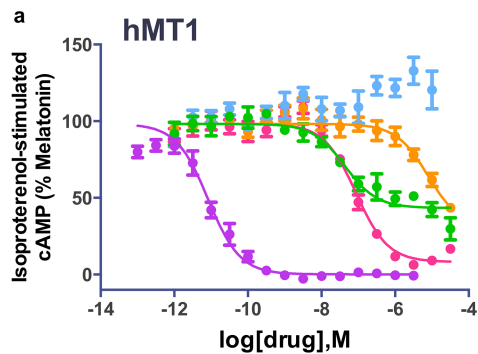
Peer review information *Nature* thanks Derk-Jan Dijk, Irina Kufareva and Ieva Sutkeviciute for their contribution to the peer review of this work.

Reprints and permissions information is available at <http://www.nature.com/reprints>.



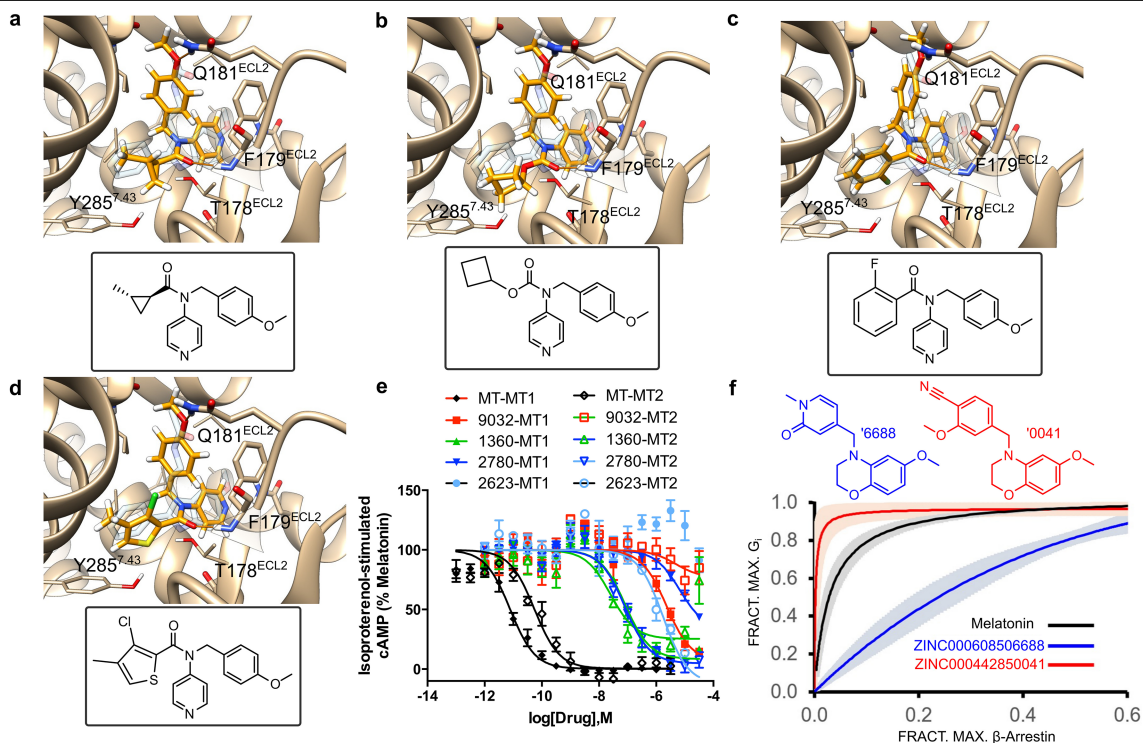
Extended Data Fig. 1 | Concentration–response curves of the initial 15 compounds in cAMP assays. a–f. Inhibition of isoproterenol-stimulated cAMP mediated by hMT₁ (a, c, e) or hMT₂ (b, d, f) in HEK293T cells by melatonin and the 15 initial compounds. Data are normalized to the melatonin response. The 15 initial compounds were split into three graphs for clarity, melatonin

response curves are the same across graphs in a, c, e and b, d, f. Data are mean ± s.e.m. of four biologically independent experiments ($n=4$) run in triplicate, unless otherwise indicated, in which case the number of biologically independent experiments is indicated in parentheses next to the compound name.



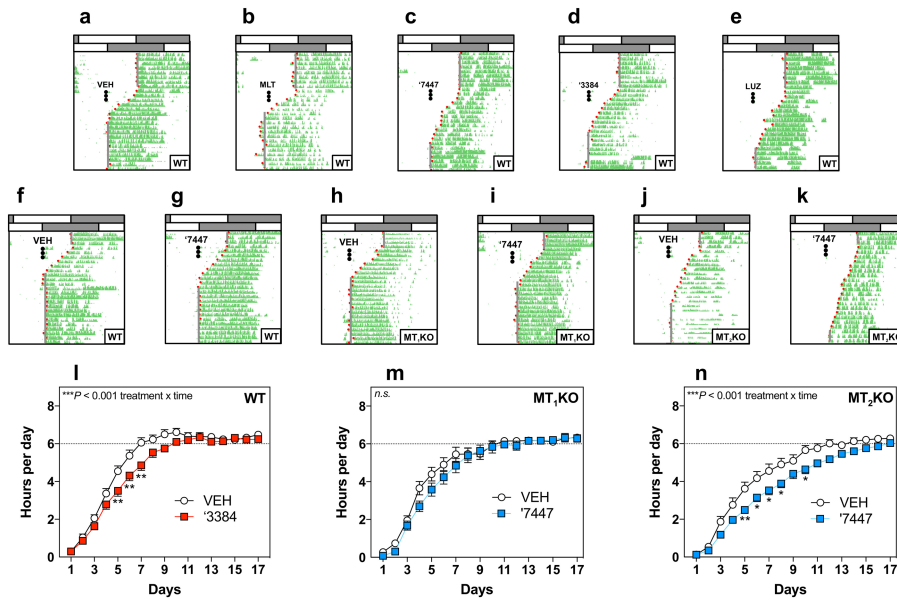
Extended Data Fig. 2 | Concentration–response curves of notable analogues based on initial hits in cAMP assays. a–f, Inhibition of isoproterenol-stimulated cAMP mediated by hMT₁ (a, c, e) or hMT₂ (b, d, f) in HEK293T cells by melatonin and select analogues. Data are normalized to the melatonin response. The compounds were split into three graphs for clarity, melatonin

response curves are the same across graphs in a, c, e and b, d, f. Data are mean ± s.e.m. of four biologically independent experiments ($n=4$) run in triplicate, unless otherwise indicated, in which case the number of biologically independent experiments is indicated in parentheses next to the compound name.



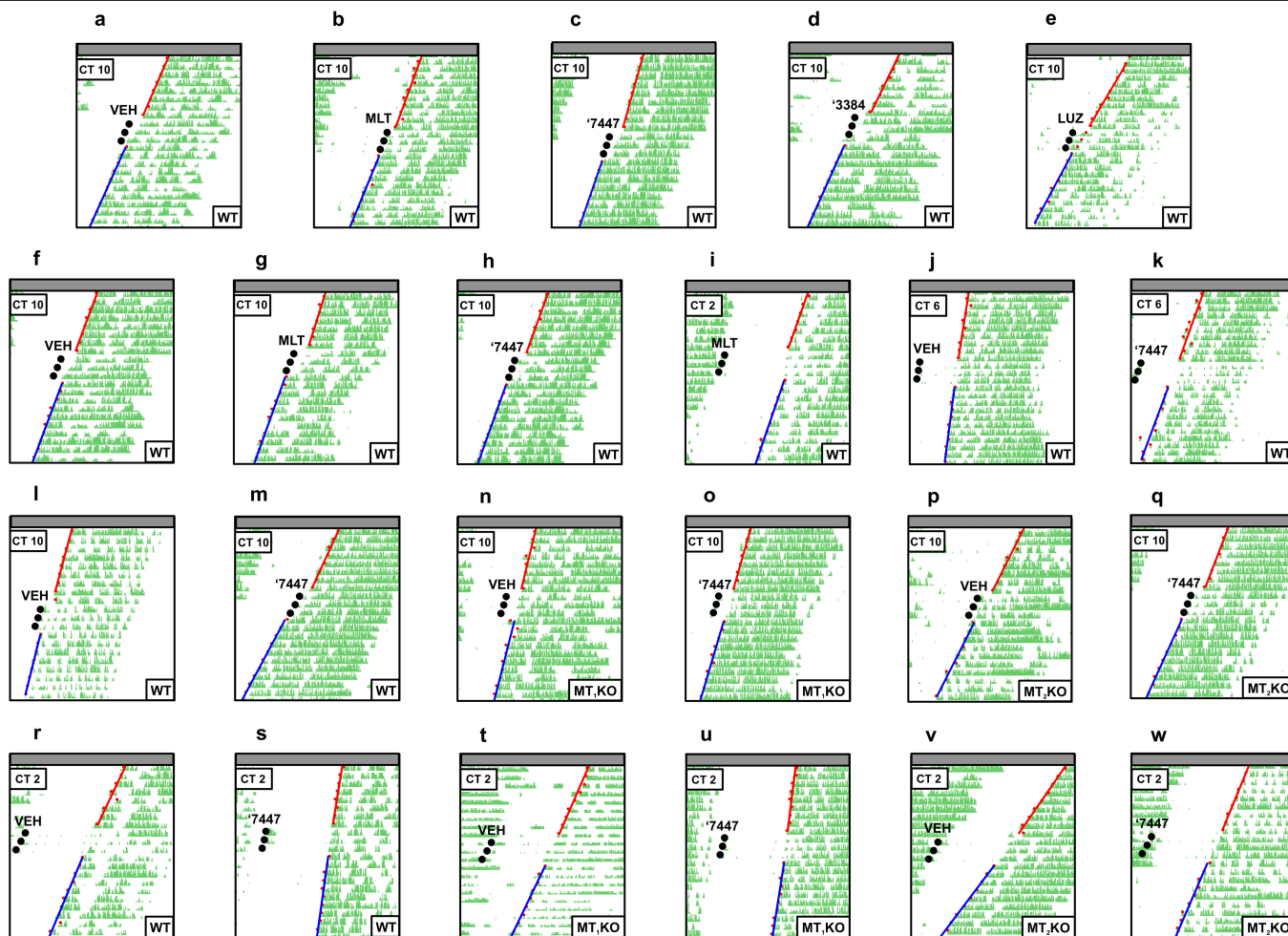
Extended Data Fig. 3 | Small changes in the ligand structure have large effects on the activity and selectivity of the melatonin receptor. **a**, Docked pose of **ZINC151209032**, an MT₁-selective direct-docking hit. **b**, Docked pose of **ZINC497291360**, a close analogue of **ZINC151209032** that has twofold selectivity for MT₂ over MT₁. **c**, Docked pose of **ZINC151192780**, an analogue for which the MT₂ selectivity increases to 89-fold over MT₁. **d**, Docked pose of **ZINC485552623**, which adds a bulkier 2-chloro-3-methylthiophene into a proposed MT₂-selective hydrophobic cleft, resulting in a fully MT₂-selective agonist without detectable MT₁ activity. All docked poses are overlaid onto the crystallographic pose of 2-phenylmelatonin in transparent blue. **e**,

Concentration–response curves of the four analogues binding to MT₁ and MT₂. Data are normalized to the melatonin response and are mean ± s.e.m. of four biologically independent experiments (*n* = 4) run in triplicate. **f**, Bias plots of **ZINC482850041** and **ZINC608506688** relative to melatonin signalling. Mean values (Supplementary Table 3) are presented as solid lines and the shading indicates the 95% confidence interval. Data in **f** are normalized to the melatonin response and represent mean ± s.e.m. of three biologically independent experiments (*n* = 3) run in triplicate, except for **ZINC608506688** for G_i activation (*n* = 4).



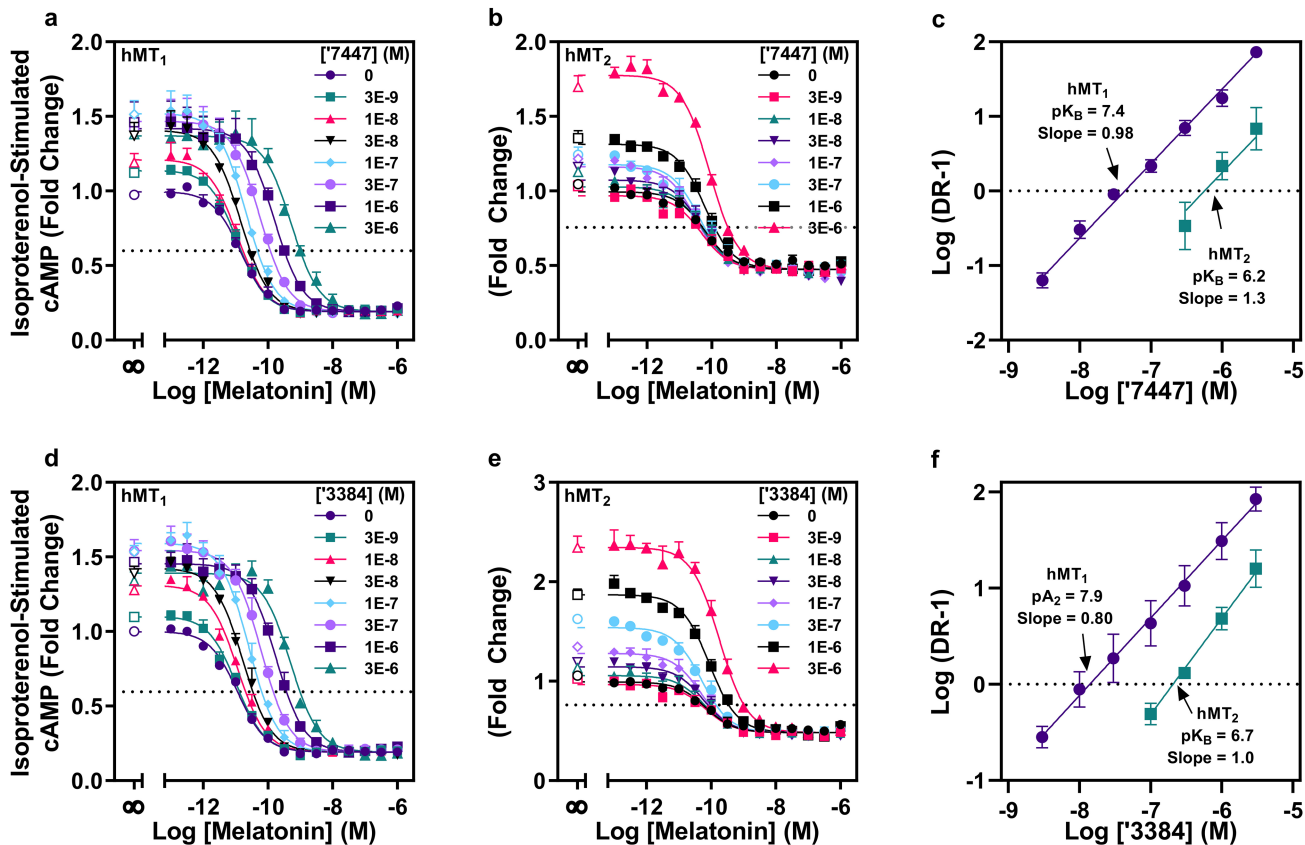
Extended Data Fig. 4 | MT_1 -selective inverse agonists decelerate the re-entrainment rate in vivo via MT_1 receptors. Data are an extension of Fig. 3a–c. **a–e**, Representative actograms of running wheel activity in wild-type (WT) C3H/HeN mice treated with vehicle (VEH) (**a**), 30 μ g melatonin (MLT) per mouse (**b**), **UCSF7447** (**'7447**) (**c**), **UCSF3384** (**'3384**) (**d**) or 300 μ g luzindole (LUZ) per mouse (**e**) immediately before the new dark onset (black dots) after an abrupt advance in the dark onset of 6 h in a 12:12 light:dark cycle (grey, dark phase; white, light phase). Compounds were administered once a day for 3 days (see Methods for additional details). **f–k**, Representative actograms of running wheel activity for C3H/HeN mice treated with vehicle (wild-type (**f**), MT_1KO (**h**), MT_2KO (**j**)) or inverse agonist **UCSF7447** (wild-type (**g**), MT_1KO (**i**), MT_2KO (**k**)) after a 6-h advance in dark onset. Mice were kept on a 12:12 light:dark cycle. **UCSF7447** (30 μ g per mouse) was administered for three consecutive days immediately before the new dark onset (black dots). **l**, The inverse agonist **UCSF3384** decelerates the rate of re-entrainment of the rhythm of running wheel activity onset in C3H/HeN wild-type mice. Data are expressed in hours advanced each day for wild-type mice treated with vehicle or **UCSF3384** (two-

way repeated-measures ANOVA; treatment \times time interaction: $F_{16,647} = 1.99$, $P = 0.0122$). **m**, The inverse agonist **UCSF7447** does not modulate the rate of re-entrainment of the onset of a running wheel activity rhythm in C3H/HeN MT_1KO mice. Data are expressed in hours advanced each day for MT_1KO mice treated with vehicle or **UCSF7447** (mixed-effect two-way repeated-measures ANOVA; treatment \times time interaction: $F_{16,474} = 1.44$, $P = 0.117$). **n**, The inverse agonist **UCSF7447** decelerates the rate of re-entrainment of the onset of a running wheel activity rhythm in C3H/HeN MT_2KO mice. Data are expressed in hours advanced each day for MT_2KO mice treated with vehicle or **UCSF7447** (mixed-effect two-way repeated-measures ANOVA; treatment \times time interaction: $F_{16,683} = 2.57$, $P = 0.000686$). Data are mean \pm s.e.m. * $P < 0.05$, ** $P < 0.01$; multiple comparisons were corrected using Tukey's post-test ($P < 0.05$). The dotted line in **l–n** indicates the new dark onset. Additional details of all statistical analyses as well as n numbers for each condition can be found in the Methods, 'Statistics and reproducibility'. All treatments were given as a subcutaneous injection.



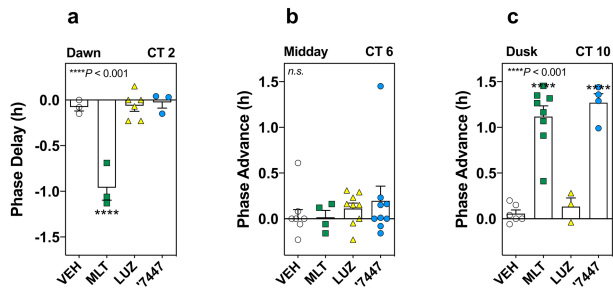
Extended Data Fig. 5 | MT_1 -selective inverse agonists induce a phase advance in circadian activity at CT 10 that is mediated by MT_1 in vivo. Data are an extension of Fig. 3d–f. **a–e**, Representative actograms of running wheel activity from individual C3H/HeN wild-type mice kept in constant dark (grey bars) treated with vehicle (**a**), melatonin (**b**), **UCSF7447** (**c**), **UCSF3384** (**d**) or luzindole (**e**). All treatments were 30 μ g per mouse except for luzindole, which was 300 μ g per mouse as described in the Methods. Mice were treated at dusk (CT 10; 2 h before the onset of running wheel activity) for three consecutive days (black dots). Red lines indicate the best-fit line of pre-treatment onsets and blue lines indicate the best-fit line of post-treatment onsets, which were both used for phase shift determinations (see Methods for more details). The corresponding quantification can be found in Fig. 3d. **f–h**, Representative actograms of running wheel activity from individual C3H/HeN wild-type mice kept in the constant dark treated with vehicle (**f**), melatonin (**g**) or **UCSF7447** (**h**; all treatments were 0.9 μ g per mouse) at CT 10. The corresponding

quantification can be found in Fig. 3d. **i–k**, Representative actograms of running wheel activity from individual C3H/HeN wild-type mice kept in the constant dark treated with melatonin (**i**) at CT 2 (10 h before the onset of running wheel activity) or vehicle (**j**) compared with **UCSF7447** (**k**; all treatments were 30 μ g per mouse) at CT 6 (6 h before the onset of running wheel activity). The corresponding quantification can be found in Extended Data Fig. 7. **l–q**, Representative actograms of running wheel activity from individual C3H/HeN wild-type (**l, m**), MT_1 KO (**n, o**) and MT_2 KO (**p, q**) mice kept in constant dark treated with vehicle (white; **l, n, p**) or **UCSF7447** (blue; **m, o, q**; 30 μ g per mouse) at CT 10. The corresponding quantification can be found in Fig. 3e. **r–w**, Representative actograms of running wheel activity from individual C3H/HeN wild-type (**r, s**), MT_1 KO (**t, u**) and MT_2 KO (**v, w**) mice kept in constant dark treated with vehicle (white; **r, t, v**) or **UCSF7447** (blue; **s, u, w**; 30 μ g per mouse) at CT 2. The corresponding quantification can be found in Fig. 3f. All treatments were given by subcutaneous injection.



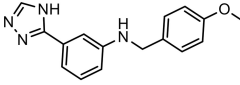
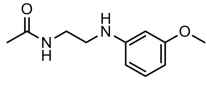
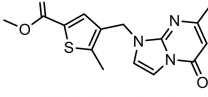
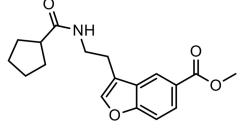
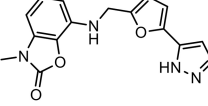
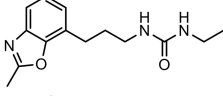
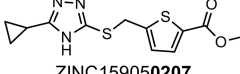
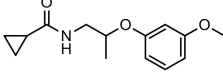
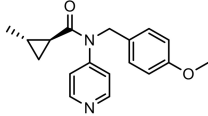
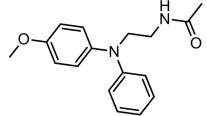
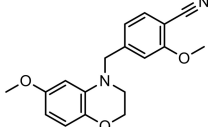
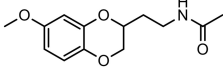
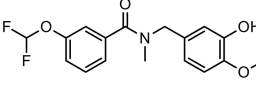
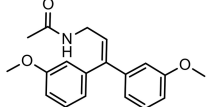
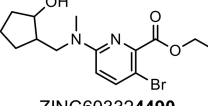
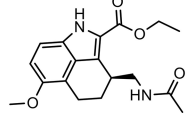
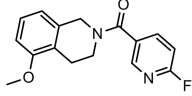
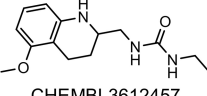
Extended Data Fig. 6 | Concentration-response curves and Schild plots of the inverse agonists UCSF7447 and UCSF3384 in cAMP assays. **a, b, d, e.** Modulation of hMT₁-mediated (**a, d**) or hMT₂-mediated (**b, e**) inhibition of isoproterenol-stimulated cAMP in HEK293T cells by melatonin in the presence of UCSF7447 (**a, b**) or UCSF3384 (**d, e**) for a range of concentrations. Data are normalized to the effect of isoproterenol alone and are mean ± s.e.m. of three biologically independent experiments ($n=3$) run in triplicate. **c, f.** Schild plots

depicting the competitive antagonism of melatonin by UCSF7447 (**c**) and UCSF3384 (**f**). Schild analysis of hMT₁ (purple) and hMT₂ (teal) show the competitive antagonism of UCSF7447 (hMT₁, pK_B = 7.4 ± 0.1, slope = 0.98 ± 0.03; hMT₂, pK_B = 6.2 ± 0.1, slope = 1.3 ± 0.4) (**c**) and UCSF3384 (hMT₁, pA₂ = 7.9 ± 0.1, slope = 0.80 ± 0.04; hMT₂, pK_B = 6.7 ± 0.1, slope = 1.0 ± 0.1) (**f**). Data are mean ± s.e.m. of three biologically independent experiments ($n=3$) run in triplicate.



Extended Data Fig. 7 | Differential phase shift profile for the inverse agonist UCSF7447 compared to the agonist melatonin and a prototype antagonist (luzindole) across the circadian cycle. a – c, C3H/HeN mice were kept in constant dark and treated with vehicle, melatonin, luzindole or UCSF7447 (all treatments were 30 μg per mouse except for luzindole, which was 300 μg per mouse, subcutaneously). Mice were treated at CT 2, 6 or 10 (10, 6 or 2 h before the onset of running wheel activity) for three consecutive days (Methods). **a,** CT 2 phase shift data were compared using one-way ANOVA ($F_{3,11} = 28.16$, $P = 1.85 \times 10^{-5}$). **b,** CT 6 phase shift data were compared using one-way ANOVA ($F_{3,26} = 0.61$, $P = 0.61$). **c,** CT 10 phase shift data were compared using one-way ANOVA ($F_{3,17} = 35.13$, $P = 1.66 \times 10^{-7}$). All multiple comparisons were made compared with vehicle using a Dunnett's post hoc test ($P < 0.05$). Values for melatonin and UCSF7447 at CT 10 were pooled from previous data for comparison to luzindole. Data are mean \pm s.e.m. **** $P < 0.0001$ for comparisons with vehicle. All treatments were given by subcutaneous injection.

Extended Data Table 1 | Active molecules from the initial docking screen

| Compound | Cluster rank ^a (global rank) | hMT ₁ ^b pEC ₅₀ (% Emax) <i>n</i> | hMT ₂ ^c pEC ₅₀ (% Emax) <i>n</i> | Tc ^d | Nearest ChEMBL23 ^e MT ₁ /MT ₂ Ligand |
|--|--|--|--|-----------------|--|
|  ZINC157665999 | 167 (197) | 4.89±0.38 (63±6) <i>n</i> =3 | Inverse 7.29±0.16 (Inverse 90±16) <i>n</i> =3 | 0.33 |  CHEMBL398017 |
|  ZINC419113878 | 396 (522) | 5.20±0.08 (84±4) <i>n</i> =4 | < 4.5 <i>n</i> =4 | 0.22 |  CHEMBL494566 |
|  ZINC433313647 | 875 (1242) | 6.81±0.32 (42±2) <i>n</i> =3 | 7.77±0.02 (96±5) <i>n</i> =3 | 0.19 |  CHEMBL125226 |
|  ZINC159050207 | 1559 (2474) | 9.00±0.15 (99±1) <i>n</i> =4 | 8.70±0.25 (83±3) <i>n</i> =4 | 0.24 |  CHEMBL1223128 |
|  ZINC151209032 | 1981 (3583) | 5.70±0.11 (88±4) <i>n</i> =4 | < 4.5 <i>n</i> =4 | 0.31 |  CHEMBL394676 |
|  ZINC442850041 | 4123 (7872) | 7.91±0.04 (99±3) <i>n</i> =3 | 9.33±0.33 (97 ± 2) <i>n</i> =3 | 0.29 |  CHEMBL344242 |
|  ZINC353044322 | 5764 (28,258) | 5.48±0.05 (87±6) <i>n</i> =4 | < 4.5 <i>n</i> =4 | 0.33 |  CHEMBL218225 |
|  ZINC603324490 | 7612 (53,767) | Inverse 5.92±0.29 <i>n</i> =3 | Inverse 6.20±0.08 <i>n</i> =4 | 0.27 |  CHEMBL3260982 |
|  ZINC182731037 | 7840 (17,095) | 5.30±0.09 (82±2) <i>n</i> =4 | < 4.5 <i>n</i> =4 | 0.29 |  CHEMBL3612457 |
| ZINC92585174 | 1836 (3010) | 7.80±0.17 (98±1) <i>n</i> =4 | 7.68±0.14 (74±8) <i>n</i> =4 | 0.23 | CHEMBL1760949 |
| ZINC432154404 | 1849 (3035) | 6.63±0.17 (95±2) <i>n</i> =4 | 7.00±0.17 (74±4) <i>n</i> =4 | 0.27 | CHEMBL1760956 |
| ZINC664088238 | 2248 (3816) | < 5 <i>n</i> =4 | 5.85±0.06 (75±8) <i>n</i> =4 | 0.20 | CHEMBL435032 |
| ZINC576887661 | 4161 (14,292) | 7.10±0.19 (83±0) <i>n</i> =4 | 7.28±0.36 (68±5) <i>n</i> =4 | 0.27 | CHEMBL491605 |
| ZINC301472854 | 5033 (10,022) | 6.03±0.10 (95±5) <i>n</i> =4 | 7.00±0.21 (88±6) <i>n</i> =4 | 0.26 | CHEMBL115444 |
| ZINC580731466 | 8503 (19,003) | 5.70±0.13 (71±3) <i>n</i> =4 | 7.55±0.10 (98±5) <i>n</i> =4 | 0.26 | CHEMBL115444 |

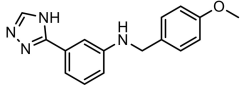
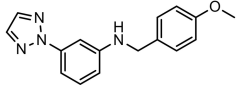
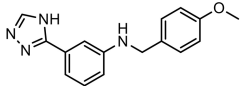
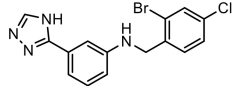
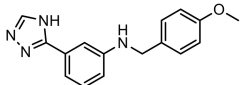
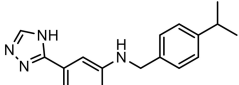
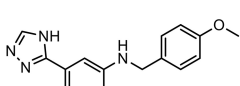
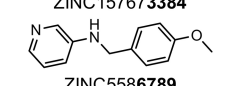
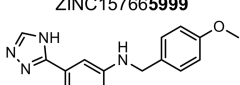
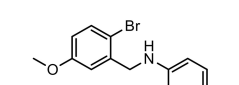
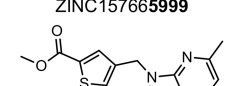
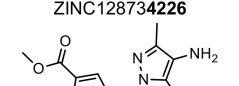
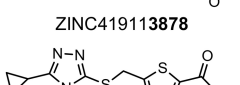
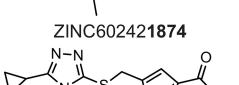
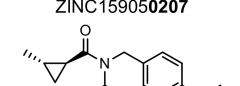
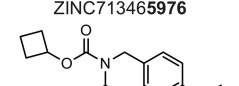
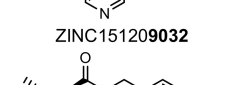
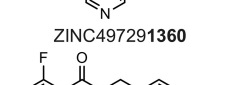
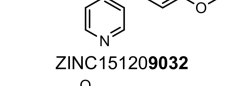
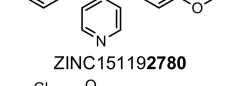
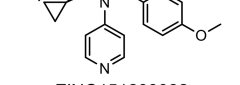
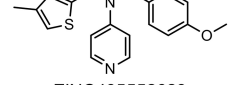
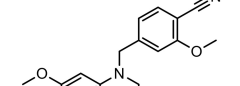
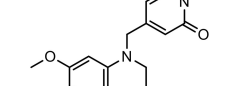
^aCluster rank and global rank are shown; the global rank is shown in brackets (Methods)

^{b,c}The log-transformed half-maximal concentration (pEC₅₀) of the inhibition of isoproterenol-stimulated cAMP production on hMT₁ or hMT₂ melatonin receptors transiently expressed in HEK293T cells. Values in parentheses represent the percentage of the maximal inhibition normalized to the percentage of the melatonin response, except for inverse agonists, which are indicated by (Inverse), for which the data are normalized to percentage of basal response induced by isoproterenol. Data represent mean ± s.e.m. of the indicated number (*n*) of biologically independent experiments run in triplicate.

^dECFP4 Tanimoto coefficient (Tc) to the most similar known MT₁ or MT₂ ligand in ChEMBL23.

^eThe MT₁/MT₂ ligand in ChEMBL23 that is most similar to the docking active molecule.

Extended Data Table 2 | Some of the potent analogues from initial hits

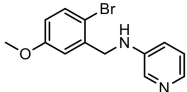
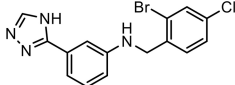
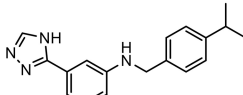
| Initial Hit ^a | Analog ^b | hMT ₁ ^c pEC ₅₀ (% Emax) <i>n</i> | hMT ₂ ^d pEC ₅₀ (% Emax) <i>n</i> |
|--|--|--|--|
|  ZINC157665999 |  ZINC864032792 | 7.49 ± 0.04 (57 ± 3) <i>n</i> =3 | Inverse 6.66 ± 0.08 (Inverse 35 ± 5) <i>n</i> =3 |
|  ZINC157665999 |  ZINC555417447 | Inverse 7.39 ± 0.10 (Inverse 62 ± 13) <i>n</i> =8 | Inverse 5.66 ± 0.10 (Inverse 84 ± 9) <i>n</i> =8 |
|  ZINC157665999 |  ZINC157673384 | Inverse 7.68 ± 0.09 (Inverse 47 ± 12) <i>n</i> =13 | Inverse 6.18 ± 0.04 (Inverse 153 ± 14) <i>n</i> =12 |
|  ZINC157665999 |  ZINC5586789 | 6.81 ± 0.72 (37 ± 8) <i>n</i> =3 | 8.07 ± 0.15 (51 ± 3) <i>n</i> =4 |
|  ZINC157665999 |  ZINC128734226 | 6.83 ± 0.17 (79 ± 3) <i>n</i> =4 | 8.15 ± 0.09 (89 ± 3) <i>n</i> =4 |
|  ZINC419113878 |  ZINC602421874 | 4.70 ± 0.11 (51 ± 3) <i>n</i> =4 | 5.35 ± 0.10 (66 ± 7) <i>n</i> =4 |
|  ZINC159050207 |  ZINC713465976 | 7.75 ± 0.22 (101 ± 0) <i>n</i> =4 | 8.23 ± 0.11 (94 ± 3) <i>n</i> =4 |
|  ZINC151209032 |  ZINC497291360 | 7.05 ± 0.10 (92 ± 2) <i>n</i> =4 | 7.48 ± 0.05 (75 ± 5) <i>n</i> =4 |
|  ZINC151209032 |  ZINC151192780 | 5.18 ± 0.22 (54 ± 4) <i>n</i> =4 | 7.13 ± 0.12 (95 ± 5) <i>n</i> =4 |
|  ZINC151209032 |  ZINC485552623 | < 5 <i>n</i> =4 | 5.80 ± 0.06 (107 ± 5) <i>n</i> =4 |
|  ZINC442850041 |  ZINC608506688 | 9.78 ± 0.13 (99 ± 1) <i>n</i> =4 | 8.60 ± 0.10 (89 ± 3) <i>n</i> =4 |
|  ZINC301472854 |  ZINC223593565 | 6.40 ± 0.18 (86 ± 4) <i>n</i> =4 | 6.45 ± 0.20 (58 ± 5) <i>n</i> =4 |

^aCompounds were selected directly from the primary docking screen and were found to be active after in vitro testing.

^bAnalogue of the initial hit.

^{c,d}The pEC₅₀ of the inhibition of isoproterenol-stimulated cAMP production on hMT₁ or hMT₂ melatonin receptors transiently expressed in HEK293T cells. Values in parentheses represent the percentage of the maximal inhibition normalized to the percentage of the melatonin response, except for inverse agonists, indicated by (Inverse), for which the data are normalized to the percentage of the basal response induced by isoproterenol. Data are mean ± s.e.m. of the indicated number (*n*) of biologically independent experiments run in triplicate.

Extended Data Table 3 | Pharmacokinetics of three melatonin receptor type-selective ligands

| Compound | pIC ₅₀ (Emax %) pEC ₅₀ (IA) | C _{max} ^a (ng/mL) | AUC ^b (hr*ng/mL) | T _{1/2} ^c (hr) | CL ^d (mL/min/kg) | V _{ss} ^e | Brain/Plasma ratio |
|---|---|--|--------------------------------|------------------------------------|--------------------------------|------------------------------|-----------------------|
|  ZINC128734226 MT ₂ -selective agonist | pIC₅₀ MT ₁ – 6.8 (48%) MT ₂ – 8.2 (80%) | 1922.8 | 282.1 | 0.29 | 117.9 | 1.11 | 1.58 (30') |
|  ZINC555417447 MT ₁ -selective inverse agonist | pEC₅₀ MT ₁ – 7.4 (IA) MT ₂ – 5.8 (IA) | 1948.6 | 494.5 | 0.27 | 67.11 | 1.11 | 3.03 (30') |
|  ZINC157673384 MT ₁ -selective inverse agonist | pEC₅₀ MT ₁ – 7.7 (IA) MT ₂ – 6.2 (IA) | 1299.6 | 563.8 | 0.32 | 58.48 | 1.38 | 1.43 (30') |

^aC_{max}, maximum concentration reached in blood plasma of mice.

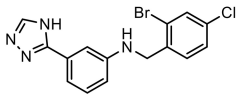
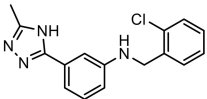
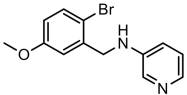
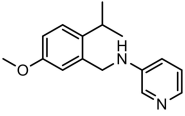
^bAUC, area under the plasma concentration-time curve.

^cT_{1/2}, half-life of the compound.

^dCL, clearance from blood plasma of mice.

^eV_{ss}, volume of the distribution at steady-state.

Extended Data Table 4 | Probe pairs of in vivo tested molecules

| Active Selective Probe (Sigma RefCode) | hMT ₁ pEC ₅₀ ^a (% Emax) <i>n</i> | hMT ₂ pEC ₅₀ ^b (% Emax) <i>n</i> | Inactive analog (Sigma RefCode) | hMT ₁ pEC ₅₀ ^a | hMT ₂ pEC ₅₀ ^b |
|---|---|---|--|---|---|
|  ZINC555417447 (SML2751) | Inverse 7.4 ± 0.10 (Inverse 62 ± 13) <i>n</i> =8 | Inverse 5.7 ± 0.10 (Inverse 84 ± 9) <i>n</i> =8 |  ZINC37781618 (SML2752) | < 4.5 <i>n</i> =3 | < 4.5 <i>n</i> =3 |
|  ZINC128734226 (SML2753) | 6.8 ± 0.2 (79 ± 3) <i>n</i> =4 | 8.2 ± 0.1 (89 ± 3) <i>n</i> =4 |  Z3670677764 (SML2754) | < 4.5 <i>n</i> =3 | < 4.5 <i>n</i> =3 |

^{a,b}The pEC₅₀ of the inhibition of isoproterenol-stimulated cAMP production on hMT₁ or hMT₂ melatonin receptors transiently expressed in HEK293T cells. Values in parentheses represent the percentage of the maximal inhibition normalized to the percentage of the melatonin response for **UCSF4226** and to the percentage of the basal activity for **UCSF7447**. Compounds were tested at concentrations up to 30 μM. Data are mean ± s.e.m. of the indicated number (*n*) of biologically independent experiments run in triplicate.

Reporting Summary

Nature Research wishes to improve the reproducibility of the work that we publish. This form provides structure for consistency and transparency in reporting. For further information on Nature Research policies, see [Authors & Referees](#) and the [Editorial Policy Checklist](#).

Statistics

For all statistical analyses, confirm that the following items are present in the figure legend, table legend, main text, or Methods section.

- | n/a | Confirmed |
|-------------------------------------|--|
| <input type="checkbox"/> | <input checked="" type="checkbox"/> The exact sample size (n) for each experimental group/condition, given as a discrete number and unit of measurement |
| <input type="checkbox"/> | <input checked="" type="checkbox"/> A statement on whether measurements were taken from distinct samples or whether the same sample was measured repeatedly |
| <input type="checkbox"/> | <input checked="" type="checkbox"/> The statistical test(s) used AND whether they are one- or two-sided <i>Only common tests should be described solely by name; describe more complex techniques in the Methods section.</i> |
| <input checked="" type="checkbox"/> | <input type="checkbox"/> A description of all covariates tested |
| <input type="checkbox"/> | <input checked="" type="checkbox"/> A description of any assumptions or corrections, such as tests of normality and adjustment for multiple comparisons |
| <input type="checkbox"/> | <input checked="" type="checkbox"/> A full description of the statistical parameters including central tendency (e.g. means) or other basic estimates (e.g. regression coefficient) AND variation (e.g. standard deviation) or associated estimates of uncertainty (e.g. confidence intervals) |
| <input type="checkbox"/> | <input checked="" type="checkbox"/> For null hypothesis testing, the test statistic (e.g. F , t , r) with confidence intervals, effect sizes, degrees of freedom and P value noted <i>Give P values as exact values whenever suitable.</i> |
| <input checked="" type="checkbox"/> | <input type="checkbox"/> For Bayesian analysis, information on the choice of priors and Markov chain Monte Carlo settings |
| <input checked="" type="checkbox"/> | <input type="checkbox"/> For hierarchical and complex designs, identification of the appropriate level for tests and full reporting of outcomes |
| <input checked="" type="checkbox"/> | <input type="checkbox"/> Estimates of effect sizes (e.g. Cohen's d , Pearson's r), indicating how they were calculated |

Our web collection on [statistics for biologists](#) contains articles on many of the points above.

Software and code

Policy information about [availability of computer code](#)

- Data collection: DOCK3.7.2
- Data analysis: GraphPad Prism 6.0, GraphPad Prism 8.0, Qniff 2.2, cheminfTools 1.0, RDKit 2015_Q3, ClockLab, MATLAB, G-power 3.0.10

For manuscripts utilizing custom algorithms or software that are central to the research but not yet described in published literature, software must be made available to editors/reviewers. We strongly encourage code deposition in a community repository (e.g. GitHub). See the Nature Research [guidelines for submitting code & software](#) for further information.

Data

Policy information about [availability of data](#)

All manuscripts must include a [data availability statement](#). This statement should provide the following information, where applicable:

- Accession codes, unique identifiers, or web links for publicly available datasets
- A list of figures that have associated raw data
- A description of any restrictions on data availability

Probe pairs are available from Sigma with the identifiers SML2751 (ZINC555417447), SML2752 (ZINC37781618), SML2753 (ZINC128734226), and SML2754 (Z3670677764). The identities of the compounds docked in this study are freely available from the ZINC database, <http://zinc15.docking.org>, and all active compounds may be purchased from Enamine. Figures with associated raw data include: Extended Data Figs. 1&2, Extended Data Table 1&2 for which further data are included in Supplementary Tables 1 (MT1 and MT2 affinities, MT1 DOCK energies/ranks) and 2 (compound purity information); Extended Data Fig. 3, for which bias information is included in Supplementary Table 3; Fig. 2, for which GPCRome screening, concentration-response curves, competition binding, and LC/MS data is included in Supplementary Data 1-5, Extended Data Fig 6, and statistical parameters in Supplementary Table 5; Supplementary Data 6&7 (synthesis routes and spectra of compounds); Fig. 3, for which further data is included in Extended Data 4-5, Supplementary Table 4, Extended Data Fig. 7.

Raw data is available for Fig 2 and Fig 3. We have also included raw data for Supplementary Data 3a-h and Supplemental Data 4a-d. Also included is raw data for Fig 3a,b,c (re-entrainment) and Extended Data Fig 4 (re-entrainment), Fig 3d,e,f (phase shift) and Extended Data Fig 7.

Field-specific reporting

Please select the one below that is the best fit for your research. If you are not sure, read the appropriate sections before making your selection.

Life sciences Behavioural & social sciences Ecological, evolutionary & environmental sciences

For a reference copy of the document with all sections, see [nature.com/documents/nr-reporting-summary-flat.pdf](https://www.nature.com/documents/nr-reporting-summary-flat.pdf)

Life sciences study design

All studies must disclose on these points even when the disclosure is negative.

| | |
|-----------------|---|
| Sample size | For phase shift and re-entrainment experiments we determined statistical power a-priori (α error probability = 0.05) based on data for a known effect size for melatonin in these paradigms (Dubocovich et al. 1998; Dubocovich et al. 2005; G-power 3.0.10). |
| Data exclusions | Individual actograms of wheel running activity were excluded from analysis based on the exclusion criteria described below, which was completed by at least two individuals blind to treatment before data analysis was started. For re-entrainment actograms exclusion criteria includes: a) low running, sporadic activity, missing wheel activity data and/or lack of entrainment; b) entrainment of running activity more than 1 h before or after the "old" or "new dark" onset; c) re-entrainment to new dark onset before administration of the third injection (entrainment to injection). For phase shift actograms exclusion criteria includes: a) low running, sporadic activity, missing wheel activity data and/or lack of free running activity rhythms; b) tau change > 0.3 h; c) at least 2 out of 3 injections occurred outside of the target pre-determined time-range for treatment (CT 1 - 3, 5 - 7, 10 - 12). Individual points were excluded from cell based data sets when meeting the exclusion criteria for the outliers Grubbs test. |
| Replication | Fig. 2(a-b): The data are the mean \pm s.e.m. from five independent assays Fig 2(c-f): Data represent mean \pm s.e.m. from the indicated number (n) of biologically independent experiments run in triplicate. Fig 3a: The data are the mean \pm s.e.m. of independent measurements in 21 (vehicle) and 28 (UCSF7447) individual mice from 2-3 independent experiments. Fig 3b: The data are the mean \pm s.e.m. of independent measurements in vehicle (n = 28) vs. melatonin (n = 21), UCSF7447 (n = 21), UCSF3384 (n = 16), or luzindole (n = 11) individual mice from 2-3 independent experiments. Fig 3c: The data are the mean \pm s.e.m. of independent measurements in WT (n = 28 vehicle; n = 21 UCSF7447), MT1KO (n = 16 vehicle; n = 16 UCSF7447), and MT2KO (n = 20 vehicle; n = 25 UCSF7447) individual mice from 2-3 independent experiments. Fig 3d: The data are the mean \pm s.e.m. of independent measurements in (left panel) - vehicle (n = 8) vs. melatonin (n = 8) or UCSF7447 (n = 13); (center panel) - vehicle (n = 15) vs. melatonin (n = 10), UCSF3384 (n = 16), or UCSF7447 (n = 15); (right panel) - vehicle (n = 6) vs luzindole (n = 3) from 2-3 independent experiments. Fig 3e: The data are the mean \pm s.e.m. of independent measurements in WT (n = 9 vehicle; n = 10 UCSF7447), MT1KO (n = 8 vehicle; n = 8 UCSF7447), and MT2KO (n = 11 vehicle; n = 9 UCSF7447) from 2-3 independent experiments. Fig 3f: The data are the mean \pm s.e.m. of independent measurements in WT (n = 8 vehicle; n = 8 UCSF7447), MT1KO (n = 6 vehicle; n = 7 UCSF7447), and MT2-KO (n = 10 vehicle; n = 13 UCSF7447) from 2-3 independent experiments. Extended Data Fig 4h-j (re-entrainment): The data are the mean \pm s.e.m. in 4h) C3H WT - vehicle (n = 28 mice#) vs. UCSF3384 (n = 16 mice#); 4i) C3H MT1KO - vehicle (n = 16 mice#) vs. UCSF7447 (n = 16 mice#); 4j) C3H MT2KO - vehicle (n = 21 mice#) vs. UCSF7447 (n = 25 mice) from 2-3 independent experiments. Ext Data Fig 6: The data represent mean \pm s.e.m. of three biologically independent experiments (n=3) run in triplicate Ext Data Fig. 7 a-c: The data are the mean \pm SEM (n value listed in Fig legend) of independent measurements in individual mice derived from two independent experiments. Extended Data Fig 7a: Data represent the mean \pm s.e.m. in 7a) CT 2 - vehicle (n = 3), melatonin (n = 3), luzindole (n = 6), or UCSF7447 (n = 3); 7b) CT 6 - vehicle (n = 8), melatonin (n = 4), luzindole (n = 9), or UCSF7447 (n = 9); 7c) CT 10 - vehicle (n = 6), melatonin (n = 8), luzindole (n = 3), or UCSF7447 (n = 4) from 2-3 independent experiments. Extended Data Table 1: The data are the mean \pm s.e.m. from three to four biologically independent experiments run in triplicate. Ext. Data Table 2: The data are the mean \pm s.e.m. from three to four biologically independent experiments run in triplicate. Ext. Data Table 3: The data are the mean \pm s.e.m. from nine animals for each compound. Ext Data Fig. 1 and Fig. 2: The data are the mean \pm s.e.m. from four biologically independent experiments run in triplicate, unless otherwise, which is indicated in parenthesis next to each compound name. Ext Data Table 4: These data are the mean \pm s.e.m. from the indicated number of biologically independent experiments run in triplicate. Ext Data Fig. 3: The data are the mean \pm s.e.m. of four biologically independent experiments (n=4) run in triplicate. Ext Data Fig 3e,f: The data are the mean \pm s.e.m. of four (panel e) and three (panel f) biologically independent experiments run in triplicate. Supplementary Data 1: Data represent mean \pm s.e.m. of a single representative biological replicate using technical quadruplicates, and a second confirmatory biological replicate (again using technical quadruplicates) was also run for each compound. For the primary binding assay, data represent mean \pm s.e.m. of 4 biologically independent experiments. Full concentration response curves represent mean \pm s.e.m. of 3 biologically independent experiments run in triplicate Supplementary Data 2: Data represent the mean \pm s.e.m. of three biologically independent experiments run in triplicate. Supplemental Data 3 (a-h): The data are the mean \pm s.e.m. from five independent assays, except for Panel g with six independent assays. Supplemental Data 4 a-d: The data are the mean \pm s.e.m. from five independent assays. Supplemental Data 4 e-f: The data represent mean \pm s.e.m. of indicated number (n) of biologically independent experiments run in triplicate. Supplemental Data 4 g: Data represent mean \pm s.e.m. of three biologically independent experiments run in triplicate. |
| Randomization | We did not apply random assignment by using a specific method like a number generator, but animals were randomly put into treatment groups. We did not use criteria to assign groups. |

Experimental treatments were not done blind, but scoring of phase shift or re-entrainment was done blind to treatment and genotype when possible.

Reporting for specific materials, systems and methods

We require information from authors about some types of materials, experimental systems and methods used in many studies. Here, indicate whether each material, system or method listed is relevant to your study. If you are not sure if a list item applies to your research, read the appropriate section before selecting a response.

Materials & experimental systems

- n/a Involved in the study
- Antibodies
- Eukaryotic cell lines
- Palaeontology
- Animals and other organisms
- Human research participants
- Clinical data

Methods

- n/a Involved in the study
- ChIP-seq
- Flow cytometry
- MRI-based neuroimaging

Eukaryotic cell lines

Policy information about [cell lines](#)

- Cell line source(s)
- Authentication
- Mycoplasma contamination
- Commonly misidentified lines (See [ICLAC](#) register)

Animals and other organisms

Policy information about [studies involving animals](#); [ARRIVE guidelines](#) recommended for reporting animal research

- Laboratory animals
- Wild animals
- Field-collected samples
- Ethics oversight

Note that full information on the approval of the study protocol must also be provided in the manuscript.